Journal of Catalysis **183,** 131–154 (1999)
Article ID jcat.1999.2390, available online at http://www.idealibrary.com on IDEAL®

Carbon-Supported Copper Catalysts

I. Characterization

A. Dandekar,[1] R. T. K. Baker,[2] and M. A. Vannice[3]

Department of Chemical Engineering, Pennsylvania State University, University Park, Pennsylvania 16802

Received October 23, 1998; revised December 17, 1998; accepted December 22, 1998

Cu crystallites dispersed on different forms of carbon, i.e., activated carbon, graphitized carbon fibers, and diamond, were prepared and characterized by CO chemisorption, N_2O decomposition, X-ray diffraction, transmission electron microscopy, temperature-programmed reduction, and diffuse reflectance Fourier transform infrared spectroscopy (DRIFTS). Both surface and bulk properties of these carbons had an impact on the dispersion as well as the reducibility of Cu. Increasing the concentration of oxygen-containing groups on the surface of the activated carbon by a nitric acid treatment prior to Cu impregnation was beneficial in terms of rendering a higher dispersion of Cu; however, Cu was better stabilized in the higher oxidation states over a high-temperature-treated activated carbon. A higher dispersion of Cu was obtained with the diamond support compared with the graphitized fibers when prepared via a wet impregnation technique, and it is attributed to the stabilization of Cu through interactive "dangling" bonds on the diamond surface. Cu dispersed by an ion-exchange method was stabilized on the graphitized fibers in two morphologically different forms: aggregates of globular particles deposited on top of graphitic basal planes and smaller crystallites at the edges of and at defects within these planes. These morphological differences changed the reducibility of these particles and also may have altered the electronic properties of these crystallites.

INTRODUCTION

Carbon materials represent a unique family of supports because of the diverse nature of the different forms of carbon and the complex functions they can perform. From the sp^2 hybridized chemical bonding in the orderly structure of graphitized carbons and disordered turbostratic carbons like activated carbon, to the sp^3 hybridized configuration in diamond, the different allotropic forms of elemental carbon possess distinct bulk and surface properties which can be altered to modify their characteristics. In the last three decades, the use of these different forms of carbons as a heterogeneous catalyst support has grown, with activated carbon perhaps being the most studied catalyst support of the three because of the versatility of properties like porosity, surface area, and chemical nature, in addition to its mechanical resistance, stability, and inertness. Comprehensive reviews and critical analyses of these aspects have already been published (1–10). The optimization of carbon surface characteristics to induce desirable interactions at the interface between the metal precursor and the support and the influence of these modifications on the morphological, adsorption, and catalytic properties of dispersed metal particles have received much attention, as indicated by the voluminous literature cited in these review articles. In addition to activated carbon, the application of two other allotropes of carbon, i.e., graphite and diamond, has also received some attention in the past few years (1, 11–46). However, whereas the morphological and electronic properties of metals dispersed on these substrates have been investigated, the consequent effects on adsorption behavior and catalytic activity have received very limited attention.

Furthermore, despite recent theoretical and X-ray photoelectron (XPS) studies that suggest changes in the electronic structure of copper deposited on carbon substrates (11–13), the number of literature reports addressing the effects of modified carbon chemistry on the properties of Cu/carbon catalysts is small (47–55). The different forms of carbon might be anticipated to have a significant influence not only on the dispersion and sintering propensity of Cu particles dispersed on their surfaces, but also on their reducibility; however, no systematic study of the properties of Cu dispersed on these forms of carbon could be found. For copper hydrogenation catalysts, three different active phases have been proposed in the literature: Cu^+, Cu^0, and a mixture of Cu^+ and Cu^0 species (56). A study in which the dispersion and reducibility of Cu are varied to thereby control the distribution of Cu surface sites seemed appropriate. Coupled with this interest to study Cu/C catalysts from the standpoint of adsorption and catalysis is an incentive to replace the commercial copper chromite catalysts

[1] Current address: Mobil Technology Company, Paulsboro, NJ 08066.
[2] Current address: Chemistry Department, Northeastern University, Boston, MA 02115.
[3] To whom correspondence should be addressed.

0021-9517/99 $30.00

which have been extensively used for industrial hydrogenation reactions (56). Consequently, Cu crystallites dispersed on different forms of carbon, i.e., activated carbon, graphitized carbon fibers, and diamond, were prepared and characterized, the effect of different surface and bulk properties of the carbons on properties of the resulting Cu catalysts was examined, and the catalytic behavior of these catalysts in crotonaldehyde hydrogenation was studied after different reduction pretreatments. A detailed characterization of the pure carbon supports used in this study has been presented elsewhere (57). This paper describes the characterization of Cu supported on these carbons by CO chemisorption, oxygen chemisorption via N_2O decomposition, X-ray diffraction, transmission electron microscopy, and temperature-programmed reduction. In addition, diffuse reflectance Fourier transform infrared (FTIR) spectroscopy (DRIFTS) was employed to probe the chemical state of surface Cu sites using subambient CO adsorption to identify oxidation states. The consequent effect on the kinetics of crotonaldehyde hydrogenation are described in a following paper (58).

EXPERIMENTAL

Carbon Supports

The activated carbon used in this study was obtained from Norit Corp (Norit A8933), designated AC-ASIS, and it had a specified surface area of 800 m^2/g. This sample was subjected to two different pretreatments to modify its surface chemistry (59, 60). A high-temperature treatment (HTT) under flowing H_2 for 6 h at 1223 K was used to remove oxygen and any sulfur impurities from the carbon surface. This sample, labeled AC-HTT-H_2, was stored in a N_2-purged glove box. The third sample, AC-HNO_3, was prepared by heating AC-ASIS in 12 N nitric acid for 12 h at 363 K, washing and filtering with water to achieve a pH of 7, and then drying overnight at 393 K. The highly graphitic carbon fibers (GF) used in this study were pitch-based commercial fibers (P-25, Amoco Performance Products). The fibers were cut and manually ground to yield a fine powder with a BET surface area of 6 m^2/g. The synthetic diamond powder (DM) was obtained from Alfa Aesar and had a BET surface area of 25 m^2/g.

Catalyst Preparation

A standard wet impregnation technique (WI) was used to prepare approximately 5 wt% Cu catalysts with all three activated carbons, the graphitized fibers, and the diamond powder. After impregnation with an aqueous solution of $Cu(NO_3)_2$, using deionized doubly distilled water, all five catalysts, i.e., Cu/AC-ASIS, Cu/AC-HTT-H_2, Cu/AC-HNO_3, Cu/DM, and Cu/GF-WI, were dried in an oven overnight at 393 K. In addition, a 1.8 wt% Cu/GF sample was prepared by an ion-exchange (IE) technique using an aqueous solution of $Cu(NO_3)_2$ and a concentrated ammonia solution according to procedures outlined elsewhere (23, 61, 62). The pH of the suspension was maintained at approximately 10 during stirring. Prior to any further characterization, the catalyst samples were pretreated *in situ* at 1 atm by flowing 40 sccm He (GHSV $\cong 100\ h^{-1}$) for 1 h at either 423, 473, 573, or 673 K, followed by reduction in 40 sccm H_2 at the same temperature for 4 h. The exact Cu content in each catalyst was determined by atomic absorption spectroscopy.

Catalyst Characterization

CO uptakes on the pretreated catalyst samples were measured at 300 K using a stainless-steel volumetric adsorption system giving a vacuum below 10^{-6} Torr at the sample (63). After the initial isotherm, the sample was evacuated at 300 K for 1 h and a second isotherm was measured to determine reversible adsorption. The H_2 (99.999% purity, MG Ind.) and CO (99.99% purity, Matheson) were made to flow through molecular sieve traps (Supelco) and Oxytraps (Alltech Assoc.) for additional purification. O_2 chemisorption on these samples at subambient temperatures as low as 143 K yielded nonreproducible results because of large uptakes on the carbon support itself; consequently this method could not be used to estimate Cu disper-sions (62).

Dissociative N_2O adsorption at 363 K was therefore used to measure metallic Cu surface sites based on the stoichiometry $N_2O_{(g)} + 2\ Cu_s^0 \rightarrow Cu_s\text{–}O\text{–}Cu_s + N_{2(g)}$ (64), where Cu_s is a surface atom. The measurements were carried out in a gravimetric apparatus with a sensitivity of 0.1 μg. After the sample was loaded in the analyzer pan, it was pretreated *in situ* before being cooled to 363 K, 10% N_2O (99.99% purity, Matheson) in Ar (99.999% purity, MG Ind.) was introduced, and the increase in weight was monitored until it asymptotically reached a steady value. The sample was then purged with Ar (99.999% purity, MG Ind.) to desorb reversibly adsorbed N_2O, and the difference between the final and initial weights represented the amount of oxygen required to oxidize the surface Cu^0 atoms to Cu^+.

X-ray diffraction (XRD) spectra were obtained *ex situ* using a Rigaku Geigerflex diffractometer equipped with a Cu$K\alpha$ radiation source and a graphite monochromator. Each sample was given the desired pretreatment and then passivated by exposure to a flowing mixture of 1% O_2 in He at 300 K for 1 h prior to handling in air during XRD measurements. Cu crystallite sizes were calculated from the linewidth at half-height of the primary Cu^0 and Cu_2O peaks using the Scherrer equation with Warren's correction for instrumental line broadening. The passivated samples were also examined in a Philips 420T transmission electron microscope at an accelerating voltage of 120 kV. The samples were dispersed ultrasonically in acetone and placed on a

400-mesh carbon-coated copper grid, and Cu particle sizes were obtained by counting 120–200 particles in each catalyst.

The temperature-programmed reduction (TPR) spectra were obtained by using a tubular quartz reactor and heating the sample from room temperature to 1173 K at the rate of 50 K/min in a 10% H_2/90% He mixture. The effluent gases were analyzed with an on-line, computer-controlled, UTI quadrupole mass spectrometer, which was used to monitor the amounts of NO and NO_2 evolved from the nitrate anion as a function of temperature.

The infrared studies were conducted with a Sirius 100 FTIR system (Mattson Instr., Inc.) using a DRIFTS cell (HVC-DPR, Harrick Sci. Corp.) that has been extensively modified to allow *in situ* treatments up to 800 K under flowing gases (65, 66). A simple inexpensive attachment designed earlier also allowed the sample cell to be cooled to subambient temperatures using liquid nitrogen and a solenoid valve (65). Ultrahigh-purity H_2, Ar, and CO (99.999% purity, MG Ind.) were further purified by passing them through separate indicating Oxytraps (Alltech Assoc.) and molecular sieve traps (Supelco), and precise gas flow rates were maintained using mass flow controllers (Tylan Corp., Model FC-260). To enhance the low signal-to-noise ratios typically obtained with carbon samples, all three activated carbon samples were diluted with CaF_2 using a CaF_2 : C ratio of 10 : 1 before loading into the DRIFTS reactor cell. The graphitized fiber samples were diluted with CaF_2 using a CaF_2 : C ratio of 5 : 1 prior to loading. In both cases, a lower dilution ratio yielded a very low signal-to-noise ratio, whereas a higher ratio lowered the spectrum resolution (57). The diamond samples were analyzed without any diluent.

After a sample was loaded into the DRIFTS cell, the cell was purged overnight with Ar to minimize additional signal damping caused by ambient moisture. The recorded interferograms typically consisted of 10,000 signal-averaged scans obtained using a postamplifier gain of 8, an iris setting of 50, and a resolution of 4 cm^{-1}. A standard procedure was used to collect the interferograms for all the catalysts. The first interferogram was that of the initial untreated sample under flowing Ar (20 sccm). The sample was then subjected to one of the desired pretreatments previously discussed and cooled to 300 K for the second interferogram. This interferogram, when Fourier transformed with that of the corresponding pretreated unloaded support as reference, yielded the spectrum of the pretreated catalyst surface. The interferogram of the pretreated catalyst was also used as the background reference for the subsequent spectra of adsorbed CO for that sample. Following this, the heating cartridge was replaced by the subambient cooling device and the DRIFTS cell was cooled to 173 K with liquid N_2. The catalyst was then exposed to a mixture of 10% CO/90% Ar for 30 min and purged with pure Ar for 30 min. Interferograms were collected under 75 Torr CO as well as after purging the catalyst sample.

RESULTS

Chemisorption

A typical set of isotherms for CO adsorption is shown in Fig. 1 for the Cu/DM catalyst; others are provided elsewhere (62). Table 1 lists the corresponding total and irreversible CO uptakes at 100 Torr on the six catalysts after pretreatment at different temperatures. For the Cu/AC-HNO_3 catalyst, increasing the reduction temperature from 423 to 573 K resulted in a decrease in both the total and reversible uptakes. However, for Cu/AC-HTT-H_2, both total and irreversible uptakes increased following an increase in the reduction temperature. In the case of Cu/DM, both the total and irreversible uptakes passed

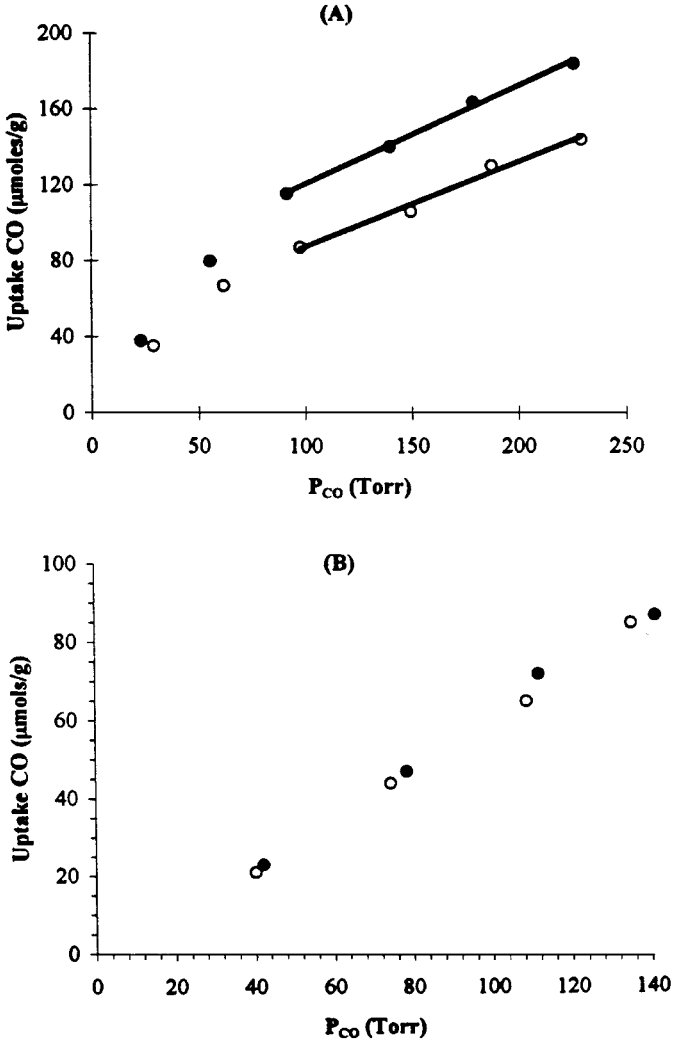

FIG. 1. CO adsorption isotherms for: (A) Cu/DM reduced at 573 K, and (B) pure DM treated at 573 K in H_2.

TABLE 1

CO Uptakes, Apparent Cu Dispersions, and Cu Particle Sizes

Catalyst	T_{red} (K)	CO uptake (μmol/g)[a]		CO_T/Cu_T	CO_{Irr}/Cu_T (Cu_s^{1+}/Cu_T)	d_{crys} (nm)	
		Total	Irreversible			d_1[b,c]	d_2[b,d]
4.8% Cu/AC-HNO_3	423	183	52	0.24	0.069	4.6	19
	473	163	25	0.22	0.033	5.4	35
	573	140	10	0.19	0.013	6.2	88
4.6% Cu/AC-ASIS	423	142	89	0.20	0.12	6.2	10
	573	130	26	0.18	0.036	7.0	34
4.9% Cu/AC-HTT-H_2	423	96	22	0.12	0.029	9.4	41
	573	102	20	0.13	0.026	8.6	45
5.1% Cu/DM	423	67	55	0.083	0.069	13.2	16
	473	74	45	0.092	0.057	12	20
	573	84	35	0.11	0.044	11	26
	673	60	10	0.076	0.012	15	91
5.1% Cu/GF-WI	423	10	5	0.013	0.0065	88	176
	473	10	7	0.013	0.009	88	126
	573	9	6	0.012	0.0077	98	147
	673	10	5	0.013	0.0065	88	176
1.8% Cu/GF-IE	423	122	25	0.44	0.082	2.7	13
	473	141	0	0.49	0	2.3	—
	573	113	0	0.39	0	2.9	—
	673	68	0	0.24	0	4.7	—
Cu Powder[e]	—	9.6	—[f]	—	—	—	—

[a] At 100 Torr.
[b] d (nm) = 1.2 (CO/Cu).
[c] Based on total CO uptake.
[d] Based on irreversible CO uptake.
[e] Cleaned in H_2 at 573 K for 1 h.
[f] No measurable uptake.

through a maximum as the reduction temperature was increased from 423 to 673 K. In comparison, both the total and the irreversible CO uptakes were low on Cu/GF-WI and did not vary much as a function of reduction temperature. In contrast, large total uptakes were obtained on the Cu/GF-IE catalyst, although no irreversible uptake was detected after reduction above 473 K. Using a 1 : 1 stoichiometry for CO_{ads} : Cu_s, where Cu_s represents a surface Cu atom (67), Cu dispersions were estimated based on both the total and irreversible CO uptakes and are reported in Table 1. It should be noted here that the reversible uptake per gram of catalyst was always higher than the reversible uptake on the pure support, which was subtracted from the uptake to provide the total uptake values in Table 1. Based on the rationale discussed earlier (67), the irreversible adsorption at 300 K can be associated with the stabilization of CO on Cu^+ sites, while the difference in the reversible uptakes on the pretreated catalysts and the respective supports can be attributed to weak reversible adsorption of CO on surface Cu^0 and residual Cu^{2+} species. The dispersion based on the total CO uptake on each catalyst, after correcting for the reversible uptake on the pure support, could provide an approximate value for total Cu surface atoms if the CO coverage on metallic Cu is high at these pressures, whereas the irreversible uptake would relate only to Cu^+ surface sites. As seen in Table 1, with AC-supported catalysts the apparent dispersions based on either of these uptakes were highest for Cu dispersed on AC-HNO_3 and lowest for Cu on AC-HTT-H_2. Cu dispersion on the DM support, although lower than that on any of the AC supports, was still much higher than that obtained for Cu/GF-WI. In contrast, apparent dispersions with the ion-exchanged Cu/GF-IE catalyst based on total CO uptake were the highest of all the catalysts, and no surface Cu^+ species were detectable after reduction at 473 K or higher.

Data obtained from N_2O decomposition on these catalysts after different pretreatments are reported in Table 2. Figure 2 represents the initial increase in the weight of the Cu/AC-HNO_3 sample (reduced at 423 K) after exposure to 75 Torr N_2O in Ar at 363 K, followed by the decrease to the final weight gain after purging with Ar at the same temperature. From the corresponding uptakes of oxygen and the assumption of a 1 : 2 stoichiometry for O_{ad} : Cu_s, dispersions of metallic Cu were calculated and are reported

TABLE 2

Oxygen Adsorption via N_2O Decomposition on Cu Catalysts at 363 K

Catalyst	T_{red} (K)	"O" uptake (μmol/g)	Cu^0/Cu_T	d_{crys}[a] (nm)
4.8% Cu/AC-HNO_3	423	110	0.280	4.0
	473	77	0.20	5.7
	573	56	0.15	7.4
4.6% Cu/AC-ASIS	423	0	0	—
	573	55	0.15	7.4
4.9% Cu/AC-HTT-H_2	423	0	0	—
	573	42	0.11	10.5
5.0% Cu/DM	423	0	0	—
	473	19	0.048	23
	573	25	0.064	18
	673	35	0.09	13
5.1% Cu/GF-WI	423	—	—	—
	473	—	—	—
	573	—	—	—
	673	—	—	—
1.8% Cu/GF-IE	423	41	0.29	3.7
	473	55	0.39	2.8
	573	64	0.45	2.4
	673	31	0.22	5.0
Cu powder[b]	—	6	—	—

[a] d (nm) $= 1.1/(2O_{ad}/Cu_T)$.
[b] Cleaned in H_2 at 573 K for 1 h.

in Table 2. Once again, the Cu^0 dispersions were dependent on both the support and the reduction temperature. The highest dispersion with any activated carbon was obtained for Cu/AC-HNO_3 reduced at 423 K. In contrast, the Cu/AC-HTT-H_2 showed no "O" uptake after reduction at 423 K, although a significant uptake was observed after reduction at 573 K. For the Cu/AC-ASIS catalyst, the uptake after reduction at 423 K was also nil, but after reduction at 573 K it was similar to that for Cu/AC-HNO_3 and higher than that for Cu/AC-HTT-H_2. In the case of Cu/DM, no significant change in the uptake was observed when reduced at or above 473 K, and the dispersions were lower than those obtained with any of the AC catalysts. No "O" uptake was detected on the Cu/GF-WI catalyst after any pretreatment, presumably because the dispersion was so low that any weight gain was within the sensitivity of the gravimetric apparatus used for the measurement. In contrast, with Cu/GF-IE, significant uptakes were observed that did not vary significantly with reduction temperatures of 473 K and above. Exposure of the pure supports to N_2O showed no significant uptakes, indicating that the increase in weight of the catalysts was due to the reaction of N_2O with surface Cu^0 species. The measurement of Cu^0 surface atoms by N_2O decomposition, therefore, should be more accurate than that obtained from the reversible CO uptake, which involved correction for uptake on the support as well as uncertain adsorption stoichiometries. However, as discussed

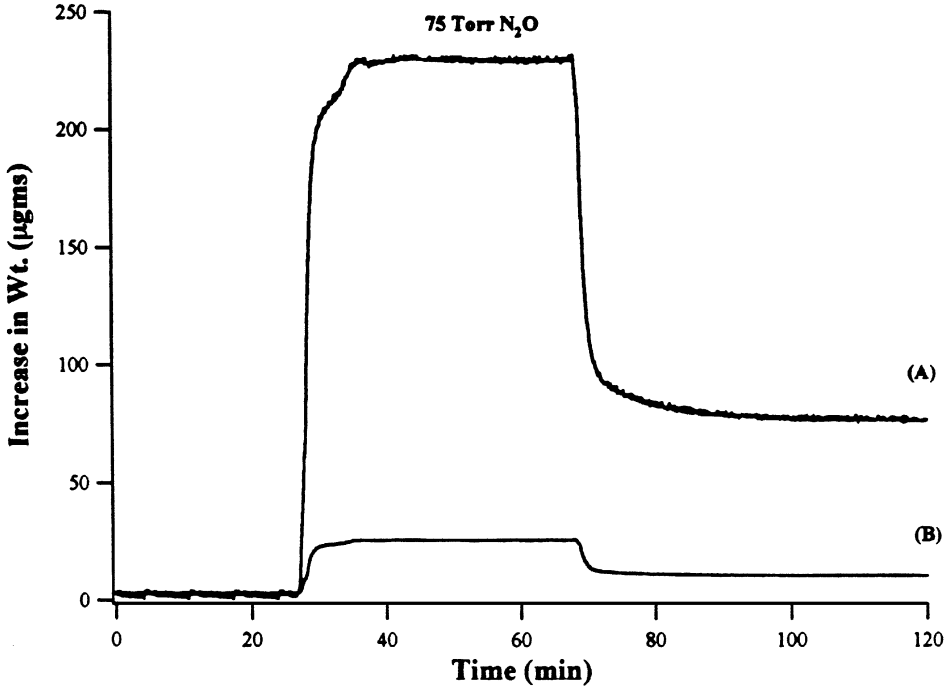

FIG. 2. Increase in weight during "O" chemisorption via N_2O decomposition at 363 K over (A) Cu/AC-HNO_3 reduced at 423 K and (B) pure AC-HNO_3 after treatment in H_2 at 423 K.

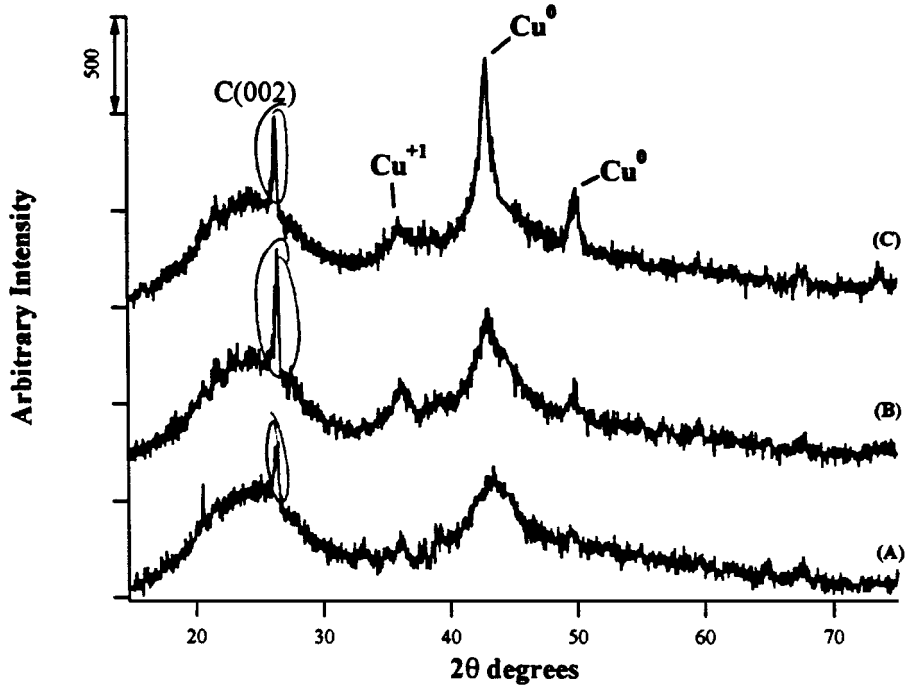

FIG. 3. XRD patterns for Cu/AC-HNO_3 after (A) He treatment at 423 K, (B) reduction at 423 K, and (C) reduction at 573 K.

in detail elsewhere (67), dispersions of Cu based on these oxygen uptakes alone represent only Cu^0 sites and do not account for any unreduced surface Cu^+ species; thus total surface Cu atoms can be underestimated using only this technique.

X-ray Diffraction

The XRD patterns for Cu/AC-HNO_3 and Cu/GF-IE after pretreatment at different temperatures, shown respectively in Figs. 3 and 4, are typical and others are provided

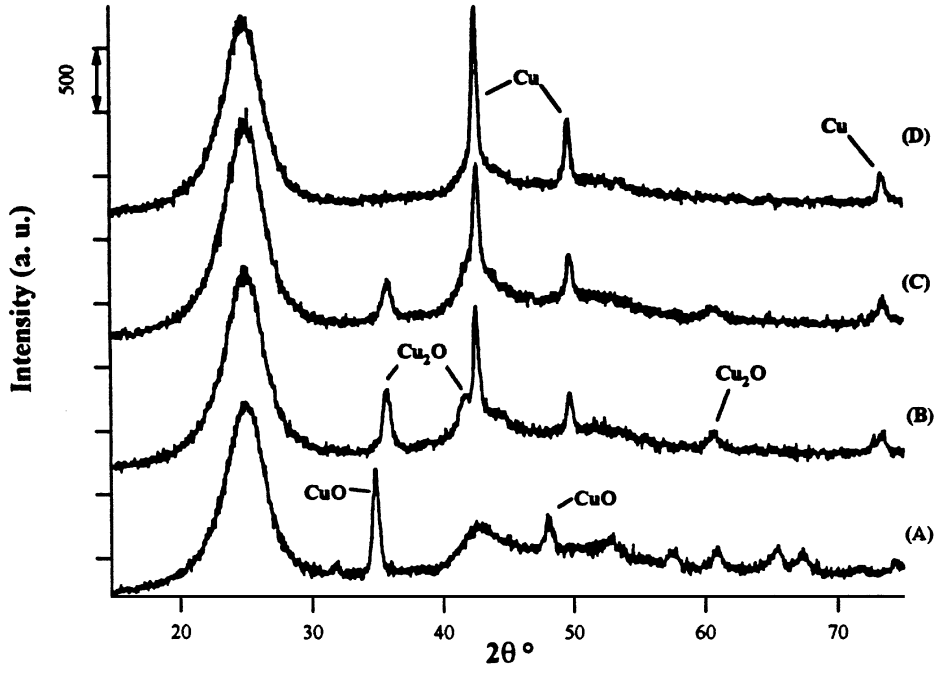

FIG. 4. XRD patterns for Cu/GF-WI after (A) He treatment at 423 K, (B) reduction at 423 K, (C) reduction at 573 K, and (D) reduction at 673 K.

TABLE 3

Average Cu Crystallite Sizes (nm) from Adsorption, XRD, and TEM Methods

Catalyst	T_{red} (K)	Adsorption		XRD		TEM		
		$(CO_{Irr}+2O_{ad})/Cu_T$	d_{surf}	Cu_2O	Cu	d_{num}	d_{surf}	d_{vol}
4.8% Cu/AC-HNO_3	423	0.36	3.2	1.3	2.9			
	473	0.24	4.9	—	—			
	573	0.16	7.2	1.1	4.9	5.6	6.4	6.7
4.6% Cu/AC-ASIS	423	0.12	6.2	9.2	5.8			
	573	0.19	7.5	6.8	7.0	8	10	11
4.9% Cu/AC-HTT-H_2	423	0.03	9.2	11	9.8			
	573	0.13	8.5	10	23	14	29	36
5.0% Cu/DM	423	0.07	12	—	—			
	473	0.11	13	13	17	13	15	19
	573	0.11	9	12	14	10	13	23
	673	0.10	13	—	18			
5.1% Cu/GF-WI	423	0.012[a]	88[a]	19	51			
	473	0.012[a]	88[a]	—	—			
	573	0.011[a]	98[a]	21	78	94	136	154
	673	0.012[a]	88[a]	—	100			
1.8% Cu/GF-IE	423	0.31	2.9	1.5	39			
	473	0.42	2.8	—	48			
	573	0.48	2.4	—	—	30	81	100
	673	0.25	5.0	—	—			

[a] Based on total CO uptake.

elsewhere (62). The peaks corresponding to the carbon supports have been analyzed elsewhere (57). Depending on the reduction temperature, broad peaks of varying intensities at 35.3°, 36.5°, and 42.9°, corresponding to the primary reflections of the CuO, Cu_2O, and Cu^0 phases, are seen in these spectra. As the reduction temperature is increased from 423 K, gradual changes occur in the peak intensities that are indicative of a progressive transition of the Cu oxidation state. The corresponding Cu crystallite sizes, based on both cuprous oxide and metallic Cu, are listed in Table 3.

Transmission and Scanning Electron Microscopy

Representative transmission electron micrographs for Cu/AC-HNO_3 and Cu/DM reduced at 573 K are shown in Figs. 5A and 6A, and the corresponding Cu particle size distributions based on approximately 120–150 particles for each are shown in Figs. 5B and 6B. Those for other catalysts are provided elsewhere (62). The number-average diameter, $d_n = \sum n_i d_i / \sum n_i$, surface area-weighted average diameter, $d_s = \sum n_i d_i^3 / \sum n_i d_i^2$, and volume-weighted average diameter, $d_v = \sum n_i d_i^4 / \sum n_i d_i^3$, of the Cu particles in each catalyst after a given pretreatment are listed in Table 3. Fairly narrow Cu particle size distributions were obtained with any of the three activated carbon supports after reduction at 573 K. The smallest Cu particles were observed on the AC-HNO_3 support, whereas the largest were seen on AC-HTT-H_2, thus suggesting a favorable influence of the oxygen-containing surface groups on the dispersion and sintering resistance of the supported Cu particles. In the case of Cu/DM, a wider distribution of particle size was seen, although the average particle sizes were comparable to those on AC-HTT-H_2. This was surprising given the huge difference in BET surface areas between the two supports, and it suggests a role of interactive stabilizing forces between the precursor and the support surface (40).

Because of the nature and texture of the graphitized carbon fibers used, instrumental limitations prevented the observation of any discernible features in the transmission electron micrographs of these Cu/GF catalysts. Only features present at the edges of the fiber fragments could be observed; consequently, the samples were also examined by scanning electron microscopy (SEM). Representative transmission electron micrographs of the Cu/GF-WI and Cu/GF-IE catalysts reduced at 573 K are shown in Fig. 7, while corresponding scanning electron micrographs of these two samples are provided elsewhere (62). The combined particle size distributions for these samples, based on both the SEM and TEM image analyses, are shown in Fig. 8. As seen in Fig. 8A, a broad distribution of much larger Cu particles occurred in Cu/GF-WI, with sizes ranging from 30 to 240 nm, whereas in Cu/GF-IE, a bimodal Cu particle size distribution existed, with maxima around 5 and 45 nm. With the latter catalyst, the larger particles were observed in the SEM images and could be attributed to excess Cu deposited on the graphitic basal planes during the

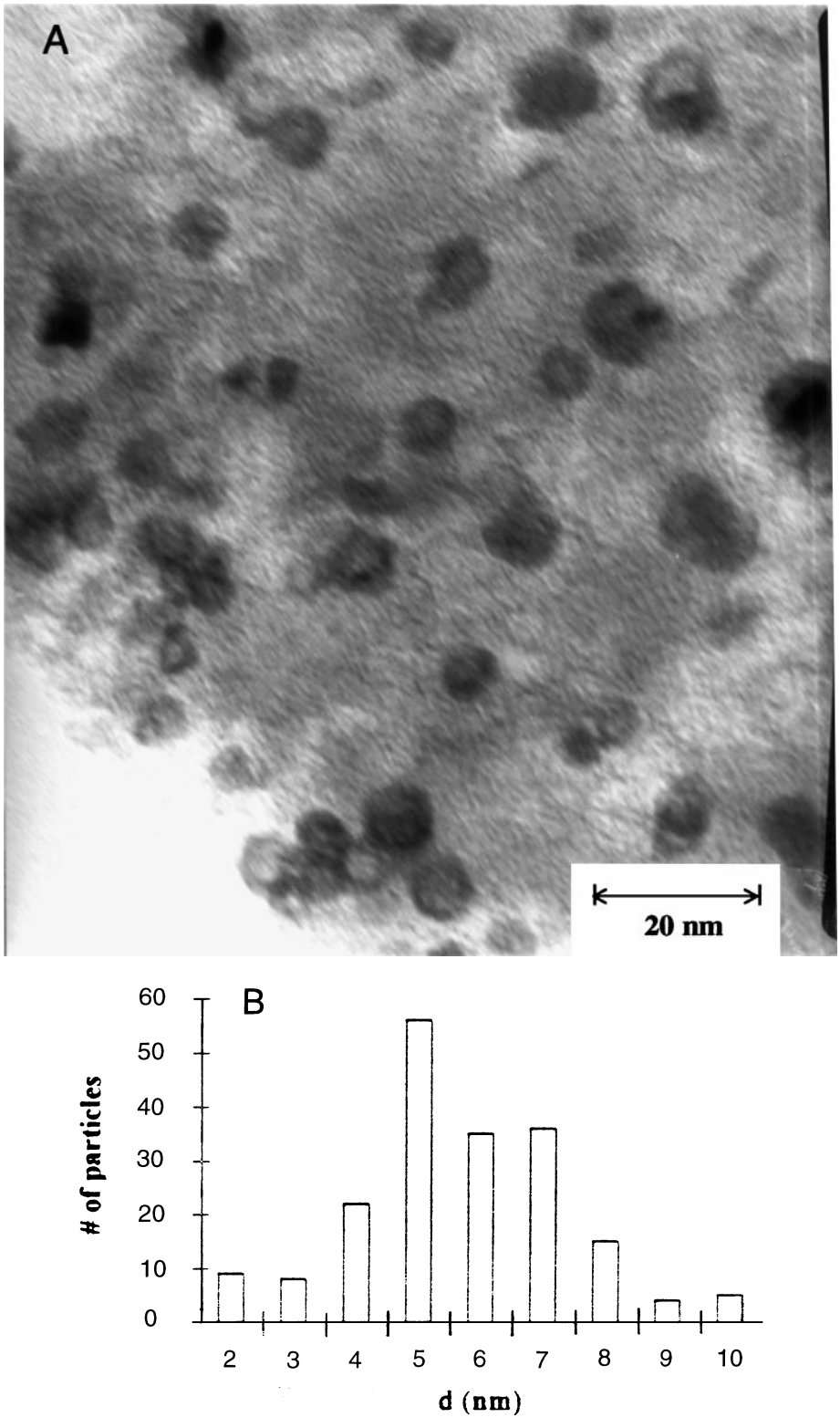

FIG. 5. (A) Transmission electron micrograph of Cu/AC-HNO_3 after a 573 K reduction. (B) Corresponding Cu particle size distribution.

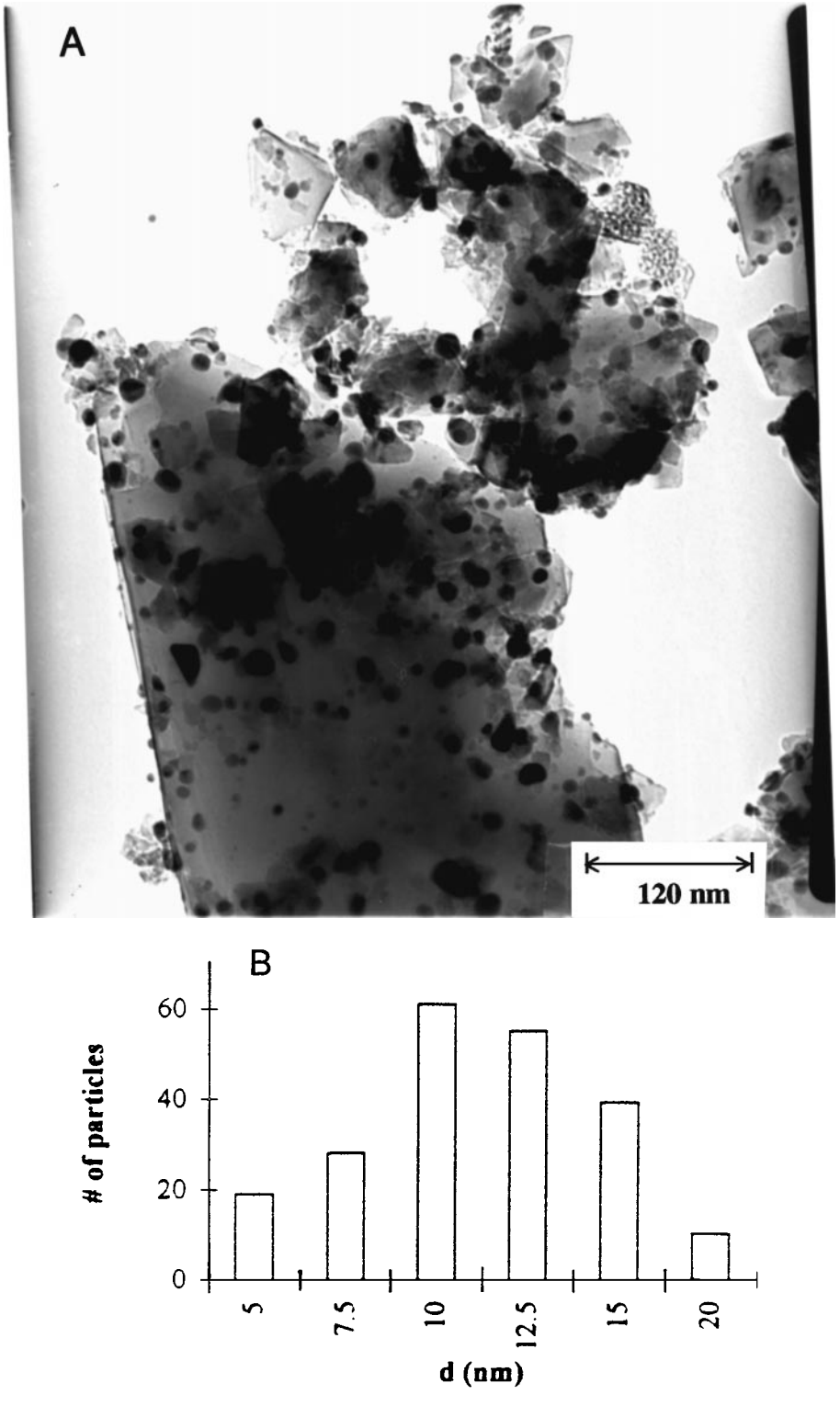

FIG. 6. (A) Transmission electron micrograph of Cu/DM after a 573 K reduction. (B) Corresponding Cu particle size distribution.

ion-exchange and/or drying procedure. Smaller particles in the range 3–6 nm can be seen located near the edges of these basal planes in the TEM images of this catalyst. It is possible that these may be decorating steps and discontinuities along the graphitic adlayers, which would be consistent with the results of Richard *et al.*, who observed a similar morphology of Pt particles deposited on a graphitized carbon by ion exchange (23–25).

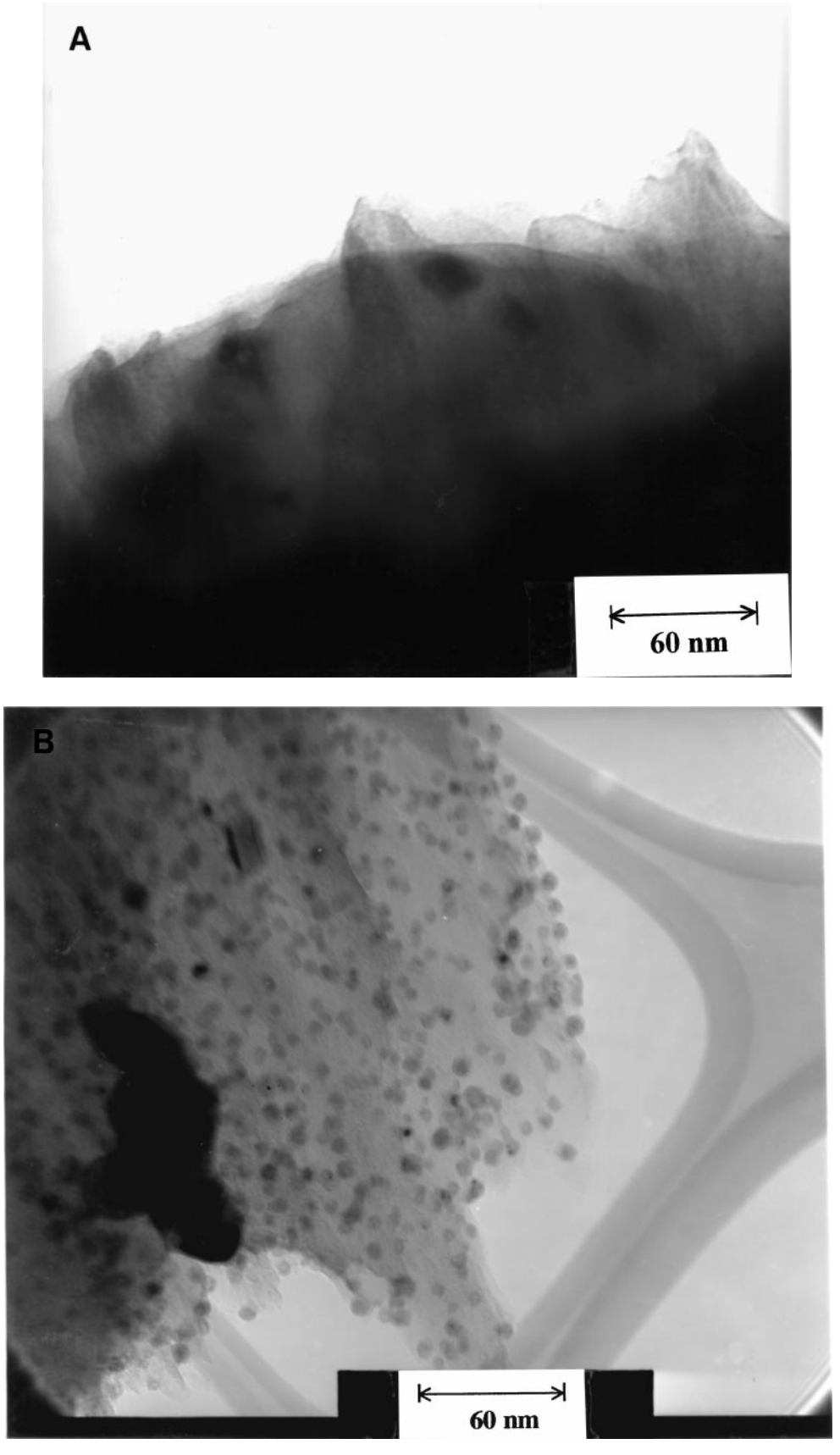

FIG. 7. Transmission electron micrographs of (A) Cu/GF-WI and (B) Cu/GF-IE after a 573 K reduction.

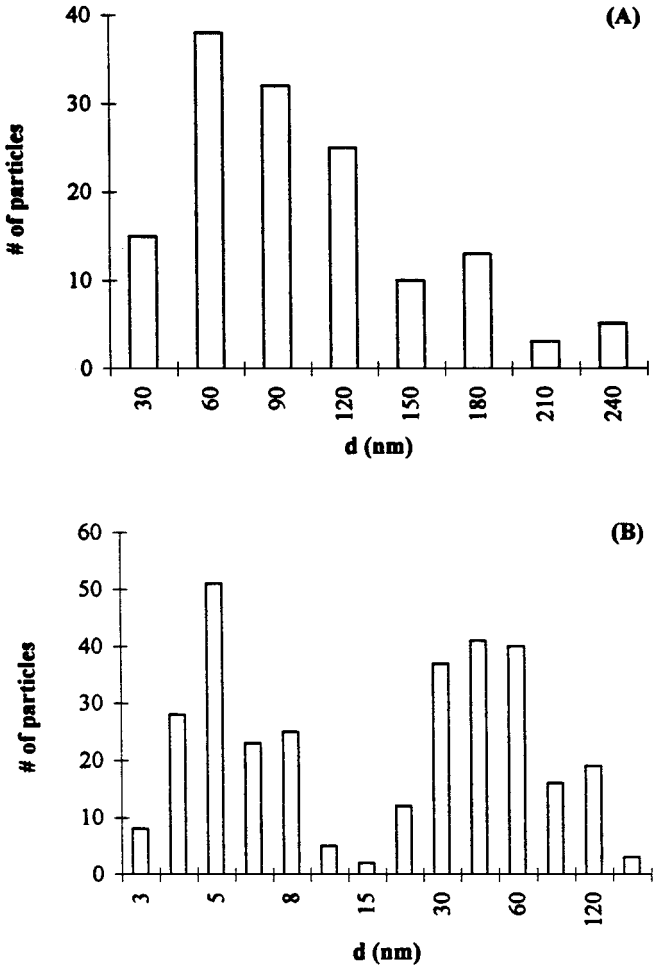

FIG. 8. Particle size distributions for Cu in (A) Cu/GF-WI and (B) Cu/GF-IE after a 573 K reduction.

DRIFTS

The FTIR spectra of the three AC-supported catalysts prior to any pretreatment are shown in Fig. 9. The reference spectra used here are those of the corresponding untreated pure supports (diluted with CaF_2). The bands in these spectra therefore essentially represent the nature of the impregnated Cu species. The spectrum of Cu/AC-HNO_3 exhibits broad overlapping bands in the region between 1200 and 1800 cm^{-1}, with peaks at 1285, 1355, 1419, 1596, 1669, and 1740 cm^{-1}, along with weaker absorbance bands at 967, 2029, and 2918 cm^{-1}. In addition, a significant drop in the absorbance intensity is seen around 3100–3500 cm^{-1}. As mentioned earlier, since the reference spectrum in this case is that of pure AC-HNO_3, this drop in intensity would imply a loss of surface functional groups present on the original carbon after interaction with Cu precursor solution. The spectrum of the Cu/AC-ASIS shows fewer absorption bands in the same region, i.e., at 960, 1245, 1355, 1419, and 1582 cm^{-1}. The spectrum of the Cu/AC-HTT-H_2 is similar to that of Cu/AC-ASIS, with weaker peaks at 960 and 1582 cm^{-1}, while the intensity of the 1355 and 1419 cm^{-1} peaks changes little. The effect of H_2 reduction at higher temperatures on the groups found on Cu/AC-HNO_3 is typified in Fig. 10. Each reference spectrum is that of the pure AC-HNO_3 after a similar treatment in H_2. Reduction at 423 K leads to a modification in the overall shape of these features, with a significant drop in intensities of all the peaks except those at 1355 and 1419 cm^{-1}, and reduction at 573 K leads to disappearance of all the bands present in the spectrum of the original catalyst. It should be noted here that along with these changes in the region 1200–1800 cm^{-1}, the negative band representing loss of intensity in the region 3100–3500 cm^{-1} slowly disappears as the reduction temperature is increased to 573 K.

The optically transparent nature of the diamond powder resulted in significantly higher signal-to-noise ratios and allowed the collection of very clean spectra of diamond-supported Cu with no dilution. The spectra of untreated Cu/DM as well as those after reduction at higher temperatures are shown in Fig. 11. Similar to the AC-supported catalysts, the untreated Cu/DM spectrum exhibits strong absorption bands at 1341 and 1423 cm^{-1} along with a broad band around 3500 cm^{-1} consisting of identifiable overlapping peaks at 3361, 3450, 3532, and 3582 cm^{-1}. In addition, weak peaks are seen at 869, 910, 1047, 1179, 2087, 2343, 2467, and 2740 cm^{-1}, and a loss in absorption intensity can be seen centered around 1744 cm^{-1}. Reduction at 423 K reduces the intensity of all bands, with those at 1047, 1341, and 1423 cm^{-1} remaining prominent. Reduction at 573 K leads to disappearance of all the significant peaks, except that at 1341 cm^{-1}, which disappears after reduction at 673 K. The negative band at 1744 cm^{-1} remains even after reduction at 673 K.

Similar spectra for Cu/GF-IE are shown in Fig. 12. Distinct peaks are seen at 1049, 1358, 1422, and 3548 cm^{-1} along with weaker ones at 791, 871, 1110, 2924, and 2964 cm^{-1} and a broad band around 3472 cm^{-1}. All these peaks are retained after reduction at 423 K, but reduction at 573 K leads to the disappearance of virtually all bands except those at 2924 and 2964 cm^{-1}. The spectra for Cu/GF-WI were not as well resolved and informative as those for Cu/GF-IE, perhaps due to the very low concentration of surface Cu species as implied by the low dispersion of Cu observed in the reduced catalyst in addition to dilution with CaF_2.

DRIFT spectra are shown for Cu/AC-HNO_3, Cu/AC-ASIS, and Cu/AC-HTT-H_2 after reduction at either 423 or 573 K, exposure to a 10% CO/90% Ar mixture at 173 K, and purging with Ar in Figs. 13 and 14, respectively. All spectra are referenced to the spectrum of the corresponding pretreated catalyst prior to CO admission. As shown in Fig. 13, after reduction at 423 K for Cu/AC-HNO_3 a distinct absorption peak developed at 2124 cm^{-1} along with a weaker but sharp peak at 2107 cm^{-1}. After reduction at 573 K, only a

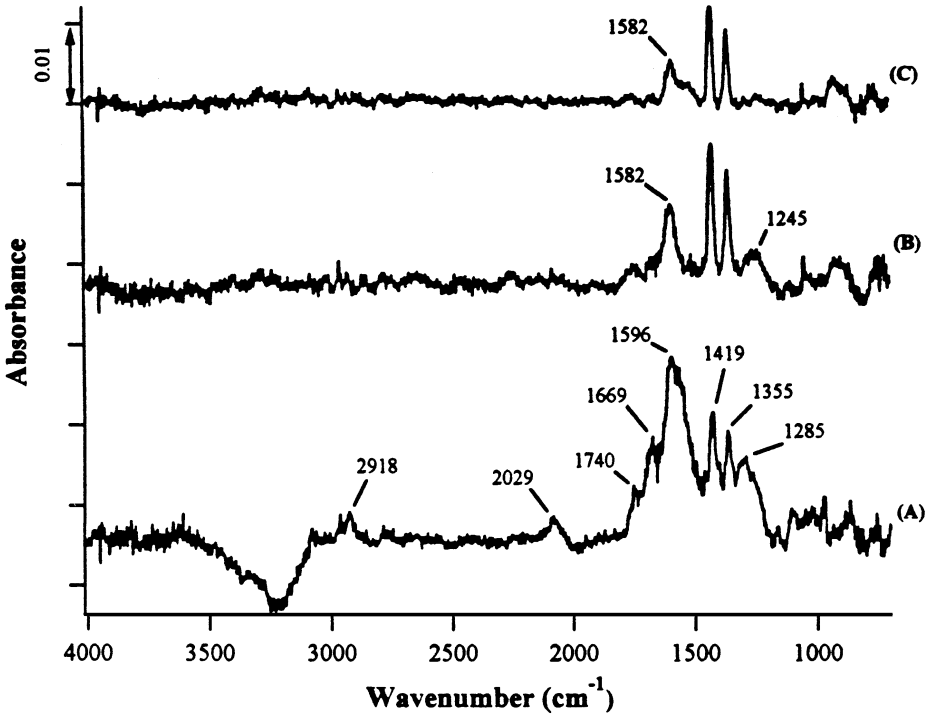

FIG. 9. DRIFT spectra of untreated Cu/AC catalysts: (A) Cu/AC-HNO_3, (B) Cu/AC-ASIS, (C) Cu/AC-HTT-H_2. Reference spectra are those of the corresponding pure carbons.

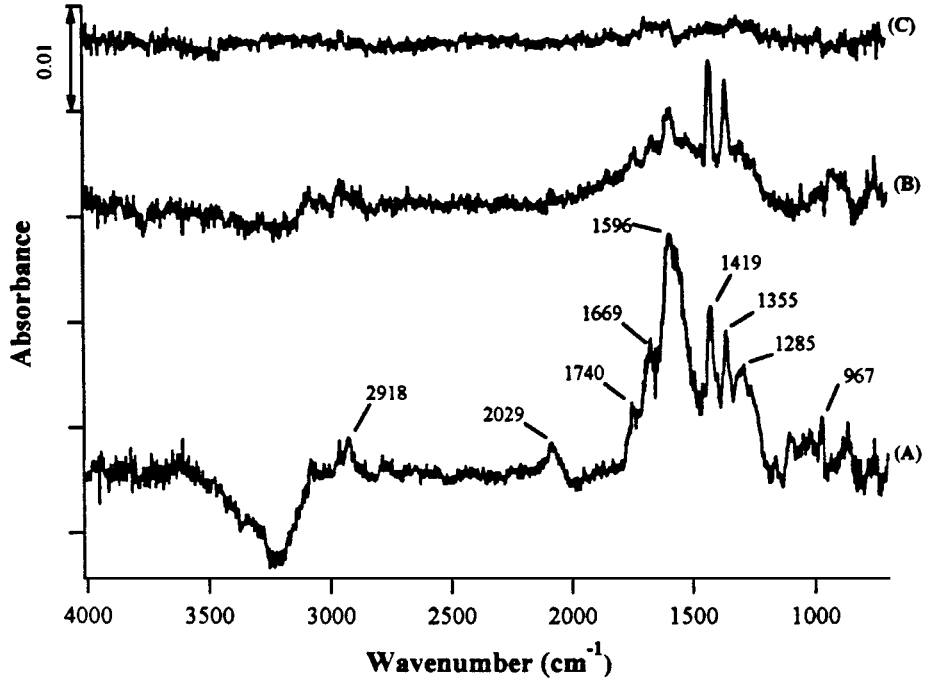

FIG. 10. DRIFT spectra of Cu/AC-HNO_3 (A) before any pretreatment, (B) after reduction at 423 K, and (C) after reduction at 573 K. Reference spectra are those of the corresponding pretreated pure AC-HNO_3.

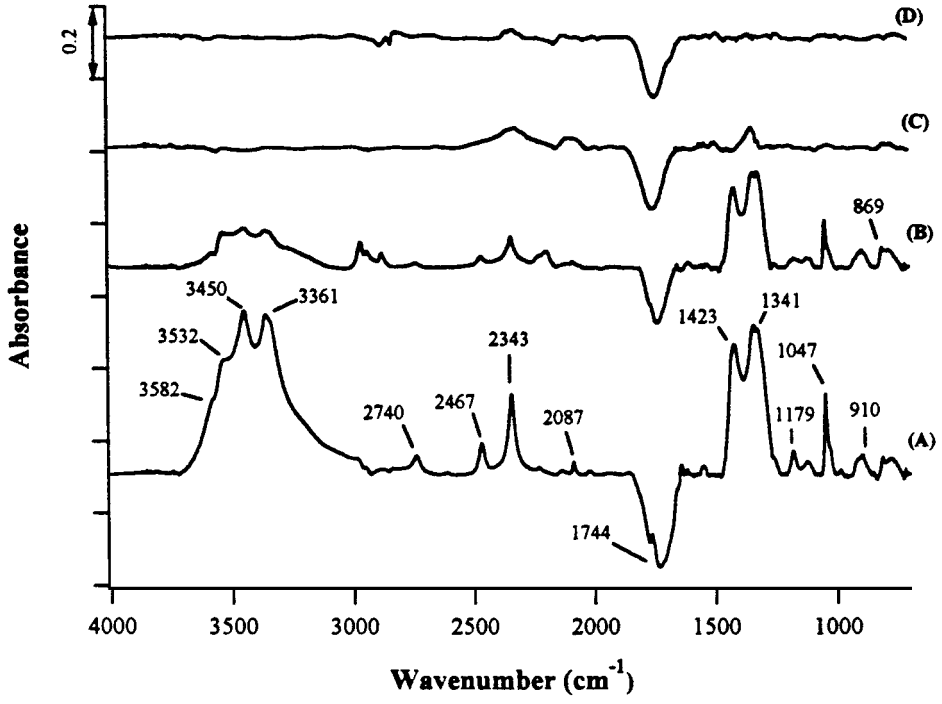

FIG. 11. DRIFT spectra of Cu/DM (A) before any pretreatment, (B) after reduction at 423 K, (C) after reduction at 573 K, and (D) after reduction at 673 K. Reference spectra are those of the corresponding pretreated DM.

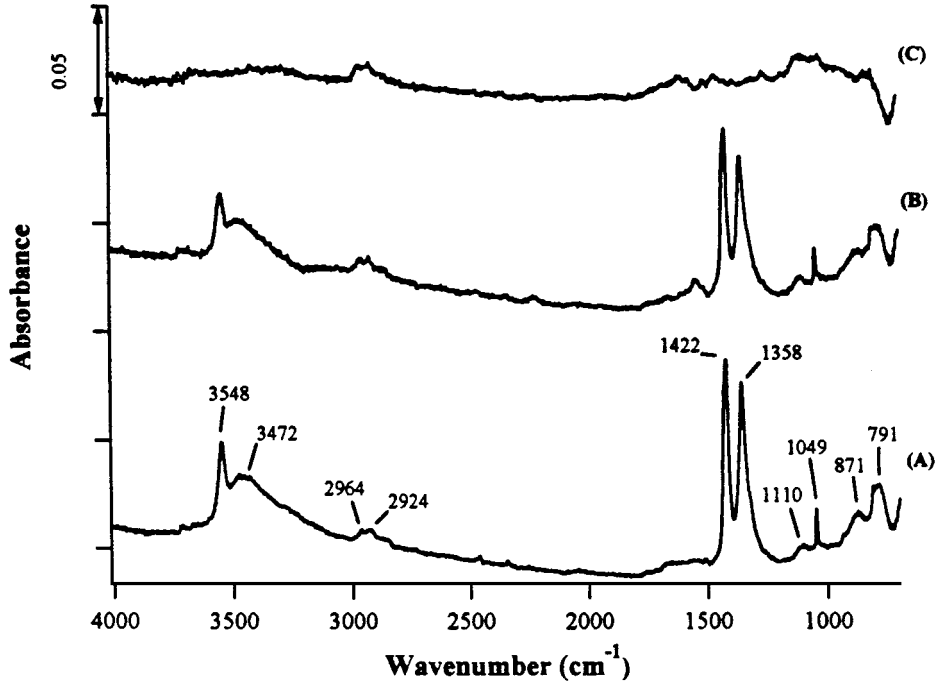

FIG. 12. DRIFT spectra of Cu/GF-IE (A) before any pretreatment, (B) after reduction at 423 K, and (C) after reduction at 573 K. Reference spectra are those of the corresponding pretreated pure GF.

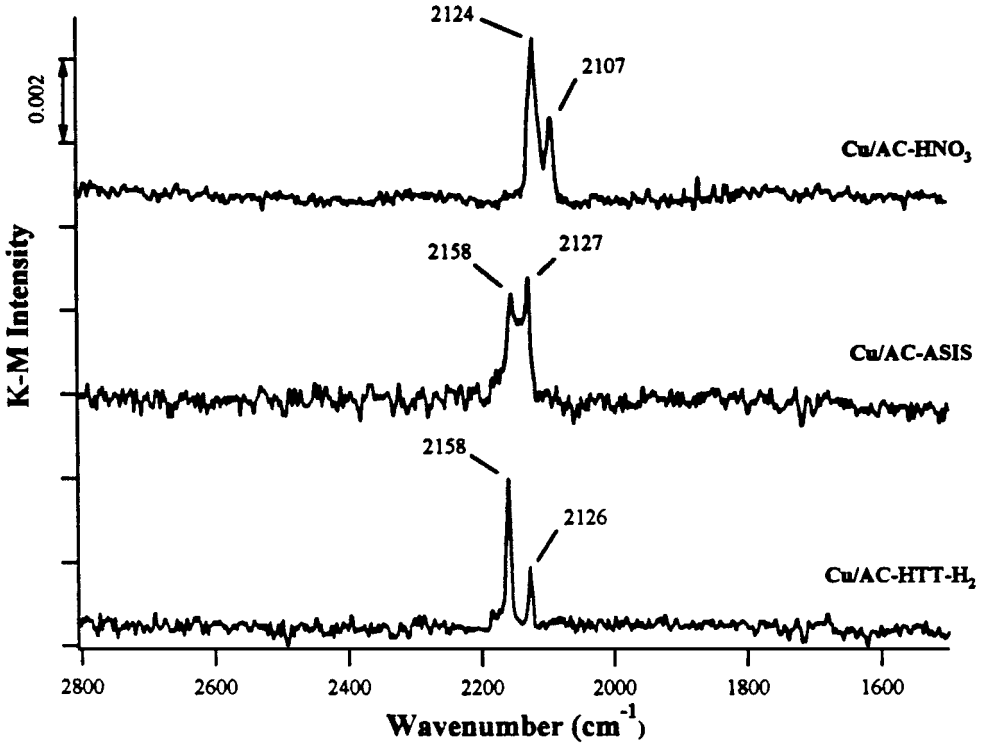

FIG. 13. DRIFT spectra of CO adsorbed on Cu/AC catalysts after reduction at 423 K; $T_{adsn} = 173$ K.

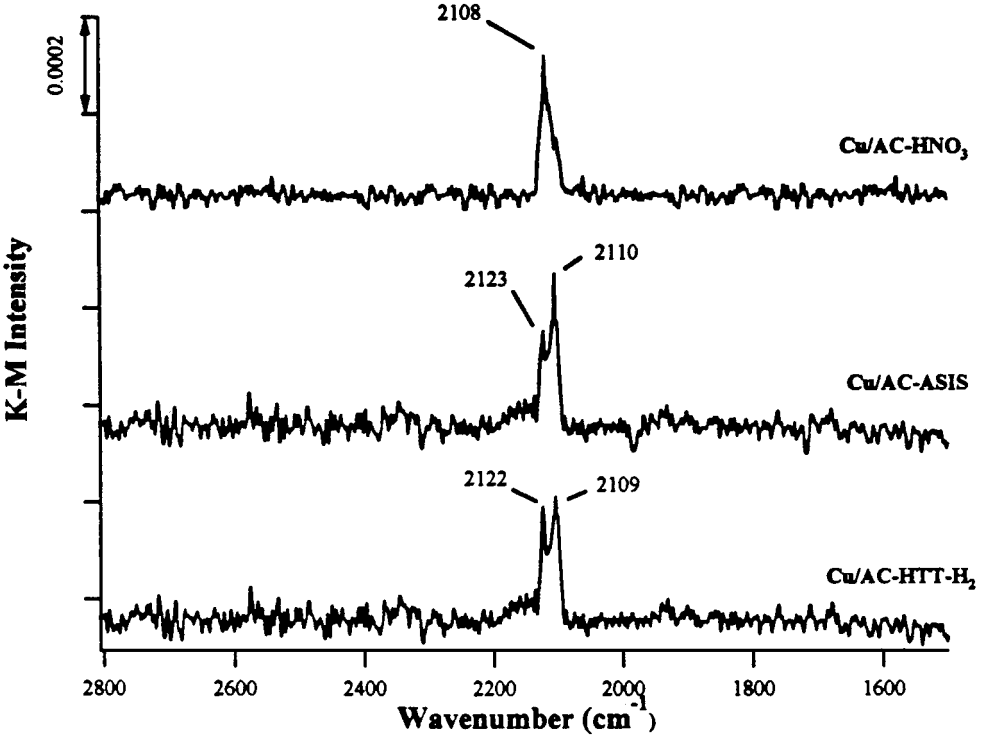

FIG. 14. DRIFT spectra of CO adsorbed on Cu/AC catalysts after reduction at 573 K; $T_{adsn} = 173$ K.

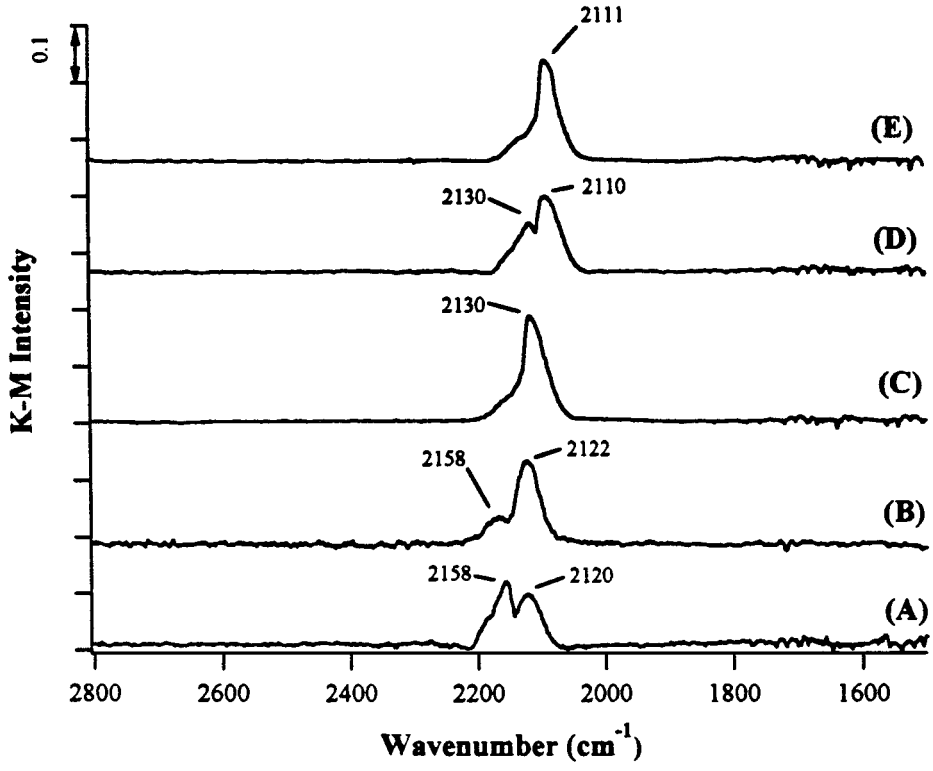

FIG. 15. DRIFT spectra of CO adsorbed on Cu/DM after (A) treatment in Ar at 423 K and reduction at (B) 423 K, (C) 473 K, (D) 573 K, and (E) 673 K; $T_{adsn} = 173$ K.

more intense band at 2108 cm^{-1} remains (Fig. 14). In contrast, the spectrum of Cu/AC-HTT-H_2 exhibits a strong absorption peak around 2158 cm^{-1} after the low-temperature treatment along with a weaker peak at 2126 cm^{-1}. After reduction at 573 K, the 2158 cm^{-1} peak disappears while that near 2122 cm^{-1} intensifies and a new sharp peak appears at 2109 cm^{-1}. The spectra for Cu/AC-ASIS exhibit intermediate features compared with those of the other AC catalysts. The absorption band at 2158 cm^{-1} corresponds to CO adsorption on Cu^{2+} sites, those from 2122 to 2127 cm^{-1} can be assigned to CO adsorbed on Cu^{+} sites, while adsorption at frequencies of 2110 cm^{-1} and below can be associated with surface Cu^{0} sites (67–69).

The DRIFT spectra of CO adsorbed on Cu/DM at 173 K after different pretreatments are shown in Fig. 15. The spectrum of the catalyst treated in Ar at 423 K for 1 h exhibits a broad band at 2158 cm^{-1} along with another one at 2120 cm^{-1}. After reduction at 423 K, the 2120 cm^{-1} peak intensifies and shifts to 2122 cm^{-1} while the 2158 cm^{-1} peak is reduced significantly. Reduction at 473 K removes the higher-frequency band and shifts the peak at 2122 cm^{-1} to 2130 cm^{-1}. Reduction at 573 K results in a decrease in the intensity of this latter peak and the appearance of a new peak at 2110 cm^{-1}. Finally, after reduction at 673 K, the 2130 cm^{-1} peak disappears and the 2110 cm^{-1} peak intensifies.

Figure 16 shows the effect of reduction temperature on the DRIFT spectra for CO adsorbed at 173 K in the Cu/GF samples. For Cu/GF-WI the results were similar to those for Cu/DM, in that treatment in Ar gives a peak at 2155 cm^{-1} with a shoulder at 2122 cm^{-1}, as shown in Fig. 16a. After reduction at 423 K, the former peak intensity drops considerably while that of the latter is enhanced. Reduction at 573 K leads to the disappearance of the 2155 cm^{-1} peak and the development of a new peak at 2092 cm^{-1}. Finally, the spectrum of the catalyst reduced at 673 K exhibits only one significant band at 2093 cm^{-1}. Corresponding spectra for Cu/GF-IE after different pretreatments are shown in Fig. 17b. The spectrum of the catalyst treated in Ar at 423 K for 1 h exhibits a strong peak at 2156 cm^{-1} and a shoulder at 2120 cm^{-1}. After reduction at 423 K, the higher-frequency peak completely disappears while that near 2120 cm^{-1} intensifies, and a new strong peak develops at 2066 cm^{-1}. Reduction at 473 K results in complete removal of the 2120 cm^{-1} band and a shift in the low-frequency peak to 2060 cm^{-1} with a significant enhancement in its intensity.

DISCUSSION

Catalyst Surface Chemistry

Characterization of the pure carbon supports used in this study using temperature-programmed desorption, XRD,

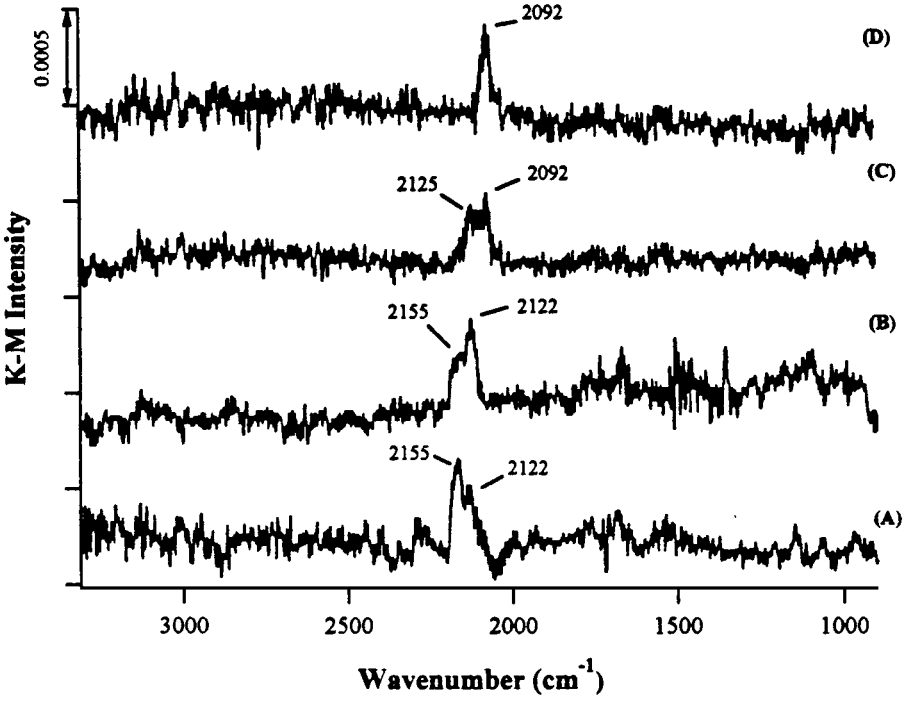

FIG. 16. DRIFT spectra of CO adsorbed on Cu/GF-WI after (A) treatment in Ar at 423 K and reduction at (B) 423 K, (C) 573 K, and (D) 673 K; $T_{adsn} = 173$ K.

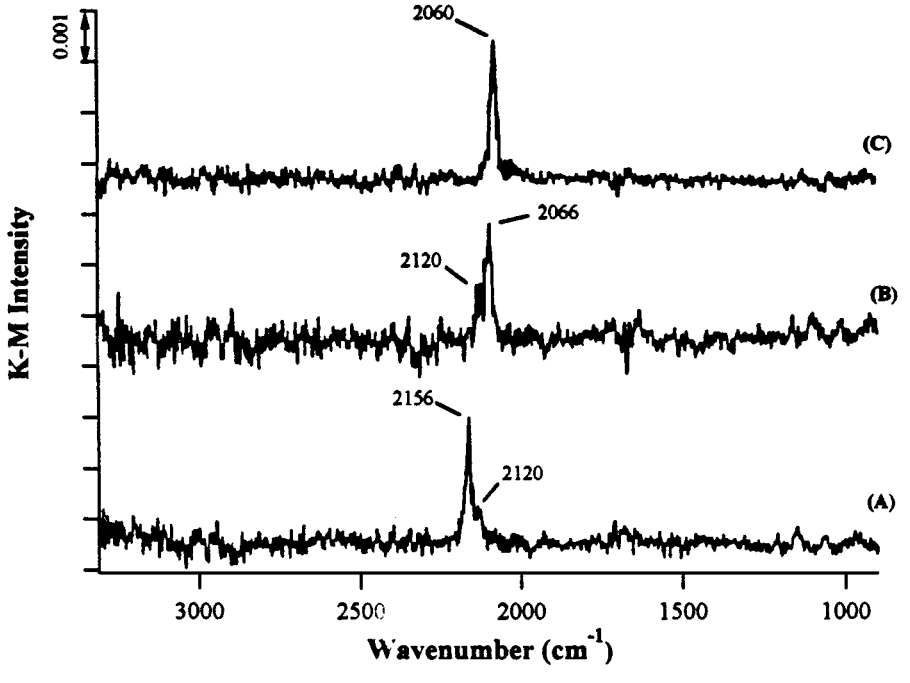

FIG. 17. DRIFT spectra of CO adsorbed on Cu/GF-IE after (A) treatment in Ar at 423 K and reduction at (B) 423 K and (C) 473 K; $T_{adsn} = 173$ K.

and DRIFTS has been discussed in detail earlier (57). Whereas all three activated carbons exhibited high BET surface areas, those of GF and DM were significantly lower. XRD patterns indicated that the structure of the graphitized carbon fibers is much more ordered compared with the turbostratic activated carbon. TPD evolution profiles of CO and CO_2 as well as DRIFT spectra of the carbons indicated that the nitric acid-treated carbon surface (AC-HNO_3) was the most acidic of all, and both strongly and weakly acidic oxygen functional groups were created on the AC-ASIS carbon following the nitric acid treatment. The spectra of the carbon pretreated in H_2 at 1223 K (AC-HTT-H_2) provided evidence for substantial amounts of chemisorbed hydrogen, presumably on highly reactive edge carbon atoms made available by the decomposition of CO-yielding complexes at temperatures above 873 K during the H_2 treatment. On the other hand, only weakly acidic or nonacidic groups were observed on the surfaces of the graphitized fiber and diamond powder. As mentioned earlier (57), characterization of pure carbon supports using IR techniques has received considerable attention during the past decade or two; however, similar studies of metal-impregnated carbon samples in the published literature are very limited. XPS studies have shown that, depending on the metal–precursor solution used and the preparation technique applied, the impregnated metal species can be stabilized in different forms on the carbon surface and changes in the functional groups present on the surface of the original carbon can also occur (70–74). One obvious way to detect these species and to identify these changes is to study the DRIFT spectra of the metal-impregnated samples using the spectrum of the unloaded carbon as the reference. Such spectra for the catalysts in this study are shown in Figs. 9–12.

The prominent band in the spectrum of untreated Cu/AC-HNO_3 (Fig. 9) can be tentatively assigned to unidentate copper carboxylate species formed on the surface of this carbon by interaction of the precursor ions with surface oxygen functionalities (75, 76). In such carboxylate salts, the C=O and C–O bonds are strongly coupled and are replaced by two equivalent carbon–oxygen bonds, resulting in a strong asymmetric CO_2 stretching vibration in the region 1575–1675 cm^{-1} and a somewhat weaker symmetric CO_2 stretching vibration around 1260–1420 cm^{-1}. Weaker overtones of these bands have been observed at lower wavenumbers for acetate, formate, and oxalate salts (75). Oxidative treatments have been reported to produce ion-exchangeable carbons, in which the protons of carboxylic acids can exchange to form complex organometallic cations (77, 78). Furthermore, binding energy shifts have been identified in XPS spectra of Cu and other metals dispersed on activated carbon which have been attributed to metal carboxylic salts and metal carbonates (70). In this study, the acidic surface groups on AC-HNO_3, introduced by the nitric acid treatment could behave in a similar fashion to anchor Cu and form the observed Cu carboxylates. The assignment of the 1596 and 1285 cm^{-1} peaks to the asymmetric and symmetric CO_2 vibrations of surface Cu carboxylate-type species therefore seems to be reasonable. The weaker bands at 1582 and 1245 cm^{-1} observed in the spectra of Cu/AC-ASIS as well as Cu/AC-HTT-H_2 can also be assigned to Cu carboxylate species on these two surfaces formed via interaction of the precursor with residual surface acidic groups.

Bands in the region 1300–1500 cm^{-1} can also be attributed to the precursor nitrate species. The asymmetric NO_3 stretch of inorganic nitrate salts absorbs strongly at 1350–1380 cm^{-1} and weakly below 1000 cm^{-1} (76). Similarly, the terminal nitro group, with two identical NO bonds, gives a strong asymmetric vibration around 1370–1470 cm^{-1} and a weaker symmetric one between 1315 and 1340 cm^{-1} (75). Based on this, the distinct peaks at 1355 and 1419 cm^{-1} in the spectra of all three untreated AC catalysts are attributed to nitrate (–NO_3) and nitrite (–NO_2) species on the carbon surface. The additional peaks at 1669 and 1740 cm^{-1} in the spectra for Cu/AC-HNO_3 cannot be assigned to absorption due to any precursor species, so based on their general position in the IR spectrum (57), they are tentatively assigned either to newly generated carbonyl (C=O) groups on the carbon surface or to enhanced absorption intensity of preexisting C=O species due to an electronic interaction with the precursor ions. The weak peak at 2918 cm^{-1} could be due to C–H stretches in these species. Because no information pertaining to this issue could be found in the literature, further justification of these assignments is not possible at this time.

The effect of pretreatment in flowing H_2 on the various surface species in Cu/AC-HNO_3 is shown in Fig. 10. After reduction at 423 K, the general shape of the bands between 1200 and 1800 cm^{-1} is modified, with a drop in the overall intensity of absorption. The peaks associated with Cu carboxylate species on the surface are much weaker, indicating a decrease in their concentration. This is consistent with the TPD of CO_2 from AC-HNO_3 which showed that the acidic groups start decomposing in H_2 at temperatures below 423 K. No significant effect on the strong peaks corresponding to –NO_2 and –NO_3 species is apparent after this treatment. Reduction at 573 K, however, completely removes these latter two strong peaks, indicating that complete decomposition of the nitrate precursor occurs between 423 and 573 K, along with the removal of all bands corresponding to Cu carboxylate species. This further supports the proposal that CO_2-yielding acidic groups are actively involved in anchoring Cu in the carboxylate form on AC-HNO_3, as compared with less acidic CO-yielding groups. The TPR spectra for NO and NO_2 desorption from Cu/AC-HNO_3, representing the thermal stability of the precursor species (62), also indicated that reduction at 573 K is sufficient to remove most of the surface nitrate and nitrite species, in agreement with the DRIFT spectra.

Similar DRIFT spectra of DM-supported Cu are shown in Fig. 11. The broad band between 3300 and 3600 cm^{-1}, with overlapping peaks at 3361, 3450, 3532, and 3582 cm^{-1}, can be assigned to –OH stretching vibrations of H_2O introduced on the DM surface during impregnation of the aqueous $Cu(NO_3)_2$ solution. This assignment is supported by the fact that these bands nearly disappear after reduction at 423 K. Prominent peaks at 1341 and 1423 cm^{-1} are attributed to asymmetric and symmetric vibrations of $–NO_3$ (nitrate) and/or $–NO_2$ (nitrite) species, as discussed earlier. As in the case of Cu/AC-HNO_3, these peaks are stable in H_2 at 423 K, but decompose on reduction at 573 K or higher. This is also verified by the TPR spectra for NO and NO_2 desorption from Cu/DM (not shown), which indicate almost complete decomposition of the precursor species during reduction at 573 K (62). Additional peaks at 2740, 2467, 2343, 1179, 1047, 910, and 869 cm^{-1}, seen in the spectrum of untreated Cu/DM, cannot be assigned to any precursor-related species. Based on their wavenumbers, the former is tentatively assigned to enhanced C–H stretches of strongly bonded surface hydrogen (76). The 1179 cm^{-1} peak could be due to the wagging motion of these C–H groups, but the 1047 cm^{-1} peak is not assigned to any particular vibration at this time. The negative band at 1744 cm^{-1} is clearly due to loss of certain functional groups originally present on the unloaded DM surface. The spectra of pure DM indicated the presence of various ketonic carbonyl groups on the surface that absorb at 1750 cm^{-1} (57); thus it is possible that some of these carbonyl species interact with Cu precursor species to anchor Cu on the surface and create a negative peak in this region.

The spectrum of untreated Cu/GF-IE in Fig. 12 exhibits strong bands at 1422 and 1358 cm^{-1} which disappear after reduction at 573 K. As in other cases, these are attributed to $–NO_2$ and $–NO_3$ precursor species. The sharp peak at 3548 cm^{-1} and the broad one at 3472 cm^{-1} can be assigned to NH and NH_2 stretching vibrations of amine and amide groups formed on the surface of the graphitized fibers (75, 76) by interaction with the ammonium hydroxide solution used to create a basic suspension for the cationic exchange of Cu. The wagging vibrations of these NH_2 bonds can be observed at 791 and 871 cm^{-1}. The retention of the 3472 cm^{-1} band after reduction at 423 K argues against its assignment to –OH groups. Similar to Cu/DM, the bands at 2924 and 2964 cm^{-1} can be assigned to stretch vibrations of surface C–H groups whose wagging modes are visible at 1110 cm^{-1}. The peak at 1046 cm^{-1}, also witnessed in the case of other catalysts, is not assigned to any particular species at this time.

Cu Dispersion

In a parallel study of Cu dispersed on a variety of supports such as DM, GF, SiO_2, Al_2O_3, TiO_2, and ZrO_2, evidence was provided that N_2O decomposition at 363 K measures only the metallic Cu surface atoms, whereas irreversible CO adsorption at 300 K is proportional to the surface concentration of cuprous ions (67). The actual dispersion of Cu should, therefore, be closer to that based on the sum of the amount of N_2O decomposed and the amount of CO irreversibly chemisorbed. That based on N_2O decomposition alone would be applicable only if all Cu species were completely reduced to Cu^0. This rationale was used here to estimate and compare the dispersion of Cu on these different carbon supports.

The effect on Cu dispersion due to pretreatment of the activated carbon prior to Cu impregnation, based on both N_2O decomposition and CO adsorption, is reported in Table 3, which lists the corresponding Cu crystallite sizes based on adsorption, XRD, and TEM analyses. From the transmission electron micrographs of these catalysts (examples of which are shown in Figs. 5–7), it can be seen that the particles tend to be relatively globular in outline on all three AC supports. The particles exist as discrete entities in all the cases, with no tendency to agglomerate to form either chains or clusters being evident. A more thorough morphological characterization of these catalysts is provided elsewhere (79). The particle size distribution and the average crystallite size, however, are strongly dependent on the support pretreatment employed. The best dispersion, obtained with Cu/AC-HNO_3, is more than twice that of Cu/AC-HTT-H_2. Since the same AC-ASIS carbon was used to prepare the AC-HNO_3 and AC-HTT-H_2 supports and an identical procedure was employed to impregnate them with Cu, the increase in dispersion can be attributed mainly to surface oxygen-containing groups introduced by the nitric acid treatment. The promotional effect of surface functionalities can be explained by the interaction between the metal precursor and the chemical state of the carbon surface during the impregnation stage (1). The removal of residual surface acidic groups during the high-temperature treatment in H_2, as evidenced by the TPD spectra (57), should increase the hydrophobicity of the original activated carbon, leading to a surface less favorable for interactions with an aqueous solvent. On the other hand, the nitric acid treatment enhances the wettability of the AC-HNO_3 carbon surface, facilitates access of the aqueous precursor solution through the internal pore structure, and results in a more homogenous distribution, giving a higher dispersion of copper (77, 80).

The maintenance of the initial metal distribution during the precursor decomposition and reduction stage has also been reported to be affected by the concentration of surface oxygen groups (77, 81). The surface oxygen groups are envisioned to act as chemical anchorage centers through the formation of some type of M–O complex on the surface, the extent of this anchoring depending on the stability of the anchoring sites and pretreatment conditions (1). The contrasting behavior of the CO_2- and CO-yielding groups on

the carbon surface has been contemplated in this context. Although no unanimously agreed on theory exists, the more acidic CO_2-yielding groups (e.g., carboxyl) are thought to be more effective catalyst dispersing sites, while the less acidic CO-yielding groups (e.g., carbonyl) are considered to be more effective for dispersion maintenance (1). For Pd/C catalysts, a higher initial dispersion was attributed to the higher acidity of the CO_2-yielding groups, which enhanced the hydrophilicity of the carbon surface and provided additional nucleation sites (77); however, the reduction temperature of 373 K was lower than that required for decarboxylation of the carbon surface. In the work by Prado-Burguete *et al*. (80), a linear correlation was reported between initial Pt dispersion and the amount of CO-yielding groups. The greater stability of the CO-yielding groups, evident from the TPD spectra, was considered to be responsible for a stronger anchorage which hindered sintering. In contrast, Coloma *et al*. (82) reported a detrimental effect of surface oxygen groups on the final dispersion of Pt/C catalysts. They argued that the carboxylic groups that act as anchoring centers during the impregnation step are decomposed during the high-temperature treatment at 773 K required to reduce Pt, which favors the surface mobility of the Pt precursor species and leads to a lower Pt dispersion. In an attempt to clarify the role of these surface functional groups on carbon, Antonucci *et al*. (83) used XPS and potentiometric titration techniques to confirm that an increase in the amounts of oxygenated species on the carbon surface decreases the platinum surface area in Pt/C catalysts. These apparently contradicting observations suggest a nonintuitive paradox of limited thermal and chemical stability of metal anchoring sites on carbon surfaces which limit the metal reduction temperature. Indeed, if the temperatures required for reducing the metal precursor and obtaining catalytic activity are beyond the stability limits of the surface groups, it would be of little consequence to use such unstable groups for anchoring the metal. In the case of copper, since complete reduction of the copper species to Cu^0 is not always desired, the effect of increasing the concentration of surface oxygen-containing groups by HNO_3 treatment appears to be beneficial in terms of rendering higher dispersion. The optimum reduction temperature for the highest activity in crotonaldehyde hydrogenation is 423 K (58) which, as is evident from the TPD data, is lower than that required for complete decomposition of CO_2-yielding groups. N_2O decomposition and CO adsorption data, however, do indicate an increase in Cu crystallite size after reduction at 573 K, which could be due to partial removal of the anchoring CO_2-yielding groups, thus leading to mobile Cu particles that could agglomerate to yield larger crystallites. From the total amounts of CO_2 and CO desorbed from the supports, which can be used as a measure of the surface concentration of these groups, a qualitative correlation can be made between the surface acidity and Cu dispersion. Both TPD and DRIFT spectra indicate that AC-HNO_3 has the highest concentration of surface anchorage sites, while AC-HTT-H_2 has the lowest. This, coupled with the dispersion data obtained from adsorption, XRD, and TEM analyses, speaks for the favorable effect of these surface groups on Cu dispersion. However, since the dispersions correlated with the total amounts of both CO_2- and CO-yielding groups, a clear distinction between the relative importance of the two types of sites cannot be made.

The much larger Cu crystallite sizes observed in the case of Cu/GF-WI, compared with Cu/AC catalysts, are consistent with the much smaller surface area of the GF support. No distinguishable Cu particles could be observed in the transmission electron micrograph of this catalyst (Fig. 7). Scanning electron micrographs of the Cu/GF-WI sample indicated the presence of predominantly circular or elliptical particles, either as remote isolated islands or as agglomerated labyrinth-type clusters, located on top of the graphitic basal planes (62). A broad size distribution of large Cu particles is observed, with particles ranging from 30 to 240 nm. In contrast, the morphology of Cu dispersed on GF by ion exchange is quite different. A scanning electron micrograph of this catalyst (62) indicated the presence of an ensemble of globular particles similar to those seen on Cu/GF-WI, with particles being relatively smaller and the size distribution ranging from 15 to 120 nm. Transmission electron micrographs of Cu/GF-IE (Fig. 7), however, indicated the presence of much smaller individual Cu crystallites along the edges of the fiber fragments, which have a much narrower size distribution. A low, fairly uniform contrast was seen at all locations, implying a predominantly flat morphology of these particles. Similar decoration of edges of graphite basal planes by Pt particles has been observed before and has been attributed to preferential stabilization of Pt along steps and edges of these planes during the ion-exchange process (23–25). In a recent study of Pt anchoring on graphite, platelets of Pt metal with a highly preferred orientation on the graphite substrate were observed, and the genesis of this structure was presumed to start via the molecular anchoring of the precursor at defect sites (33, 34). A similar interaction could be responsible for the peculiar particle size distribution of Cu in the case of Cu/GF-IE. This bimodal distribution is consistent with the chemisorption data and XRD patterns of this catalyst; i.e., the chemisorption data predict the presence of small Cu particles whereas the sharp narrow peaks corresponding to Cu^0 in the XRD patterns indicate the existence of much larger Cu particles. Thus Cu dispersed by an ion-exchange method is stabilized on the graphitized fibers in two morphologically different forms: aggregates of large globular particles deposited on top of graphitic basal planes and significantly smaller crystallites at the edges and defects within these planes. These morphological differences could have a distinct effect on the electronic properties of these

crystallites and affect their reducibility, as discussed in the next section.

The chemistry of Cu deposited on the diamond support is unique in its own way. Transmission electron micrographs of this catalyst reveal Cu particles of a fairly uniform morphology (Fig. 6). Despite the surface area of DM being similar to that of the graphitized fibers, the average crystallite size of Cu on DM is much smaller than that obtained by impregnation of GF. Enhanced stability of Cu particles on DM has been shown before, both experimentally and theoretically (40, 41), to be related to the interaction of Cu with surface "dangling bonds." The surface chemistry of diamond has been discussed in some detail (57), and free valences with dangling bonds have been proposed to exist on the edges and corners of diamond crystals as well as (100) and (111) crystal planes. The loss of intensity for Cu/DM at 1750 cm^{-1} (Fig. 11) perhaps indicates the stabilization of Cu through carbonyl group functionalities on the DM surface. A theoretical investigation of the electronic structure of copper–diamond interfaces indicates that Cu can be anchored in two basic geometries: Cu on top of a surface C atom and Cu in a fourfold coordinated position above C atoms (41). In the former case, when Cu is positioned on top of a dangling bond, a reasonably strong covalent bond is formed between the Cu 4*s* orbital and the C dangling bond, with minimal participation of the Cu 3*d* band. In the latter case, a weaker interaction with a greater participation of Cu 3*d* electrons was predicted with neighboring dangling bonds, leading to a more effective metallic type of bonding. In either case, the adhesion between Cu and diamond was predicted to be much higher than that between Cu and graphite. The higher dispersion of Cu observed on DM, compared with that on GF prepared by wet impregnation, is consistent with these theoretical predictions. Similar adhesion owing to an electronic interaction is observed between Cu and graphitic basal planes when Cu is deposited via cationic exchange on edges, adlayers, and defects of these planes.

It should be noted here that in all the above cases, Cu crystallite sizes based on both O and CO uptakes are in much better agreement with those obtained from TEM and XRD than those based on "O" uptake alone.

Distribution of Cu Oxidation States

As indicated earlier, the use of different carbon supports with varying surface and bulk properties can have a significant impact on the reducibility of dispersed copper species. Both the DRIFT spectra of CO adsorption on the pretreated catalysts (Figs. 13–17) and the XRD patterns clearly illustrated this effect. Furthermore, the relative amounts of irreversibly adsorbed CO and "O," which represent the surface concentrations of Cu^+ and Cu^0 species, respectively, also illustrate the same influence. The surface Cu species in these catalysts can exist in either the cupric (Cu^{2+}), cuprous (Cu^+), or metallic (Cu^0) form, and it was observed in most cases that Cu existed in more than one oxidation state. This distribution of surface Cu oxidation states was dependent on both the reduction temperature and the carbon support used to disperse Cu, as reduction time was held constant at 4 h. In an attempt to quantify this effect, the fraction of Cu in each valence state was estimated for each catalyst as a function of reduction temperature. For the DRIFT spectra of adsorbed CO, it was assumed that each fraction was proportional to the area under the deconvoluted peak corresponding to each individual oxidation state. With the XRD patterns, the absolute intensities were used for these fractions, which represent bulk compositions. Regarding the chemisorption data, the amounts of CO and "O" irreversibly adsorbed directly yielded the total surface concentrations of Cu^+ and Cu^0 sites, respectively. If it is then assumed that the total CO uptake on Cu at 300 K and 75 Torr (obtained after correcting for the reversible uptake on pure supports) approximates the surface concentration of Cu in all three oxidation states, the surface concentration of Cu^{2+} species can be estimated by subtracting those of Cu^+ and Cu^0 from the total uptake. The corresponding fractions—$\theta_{Cu^{2+}}$, θ_{Cu^+}, and θ_{Cu^0}—obtained from the three characterization techniques are listed in Table 4 for all catalysts.

The strongly adsorbed CO species 2124 cm^{-1} on Cu/AC-HNO_3 reduced at 423 K provides evidence for the presence of Cu^+ species on the surface along with metallic Cu, which adsorbs CO giving a peak at 2107 cm^{-1}. The disappearance of the former peak after reduction at 573 K, which parallels an enhancement in the intensity of the latter peak, clearly indicates complete reduction to metallic (Cu^0) copper. In contrast, the copper species dispersed on AC-HTT-H_2 seem to be more difficult to reduce at lower temperatures, as testified by the strong peak at 2158 cm^{-1}, corresponding to CO on unreduced Cu^{2+} species, in addition to that at 2126 cm^{-1} for Cu^+ species after reduction at 423 K. After reduction at 573 K, a considerable coverage of Cu^+ species remains along with metallic copper. A similar transition in the Cu oxidation states as a function of reduction temperature as well as the pretreatment of the activated carbon is observed in the XRD patterns of these catalysts. As seen in Table 4, the fractions of Cu present in different valence states, as estimated by all three techniques, are typically quite consistent with each other and show that Cu on AC-HNO_3 reduces more easily than Cu on AC-HTT-H_2 at lower reduction temperatures. This observation, coupled with the fact that Cu dispersion on AC-HNO_3 is more than twice that obtained on AC-HTT-H_2, perhaps implies that smaller Cu particles are easier to reduce. This is in agreement with a previous study on Cu reducibility by Robertson *et al.* (84) which showed that highly dispersed CuO/SiO_2 was reduced at a much lower temperature than unsupported CuO. The effect observed in the

TABLE 4

Distribution of Cu Oxidation States in Cu/Carbon Catalysts

Catalyst	T_{red} (°C)	Chemisorption			DRIFTS: CO adsorption at 173 K			XRD		
		$\theta_{Cu^{2+}}$	$\theta_{Cu^{+}}$	$\theta_{Cu^{0}}$	$\theta_{Cu^{2+}}$	$\theta_{Cu^{+}}$	$\theta_{Cu^{0}}$	$\theta_{Cu^{2+}}$	$\theta_{Cu^{+}}$	$\theta_{Cu^{0}}$
4.8% Cu/AC-HNO_3	423	0	0.19	0.81	0	0.60	0.40	0	0.24	0.76
	473	0	0.14	0.86	0	0.11	0.89	—	—	—
	573	0	0.08	0.92	0	0	1.0	0	0.11	0.89
4.6% Cu/AC-ASIS	423	0.37	0.63	0	0.40	0.60	0	0.22	0.31	0.47
	573	0	0.19	0.81	0	0.28	0.72	0	0.20	0.80
4.9% Cu/AC-HTT-H_2	423	0.77	0.23	0	0.70	0.30	0	0.36	0.30	0.34
	573	0	0.19	0.81	0	0.39	0.61	0	0.18	0.82
5.0% Cu/DM	423	0.32	0.68	0	0.15	0.85	0	0.63	0.37	0
	473	0	0.54	0.46	0	0.78	0.22	0.19	0.31	0.60
	573	0	0.41	0.59	0	0.38	0.62	0	0.27	0.73
	673	0	0.13	0.87	0	0	1.0	0	0.12	0.88
5.1% Cu/GF-WI	423	0.5[a]	0.5[a]	0[a]	0.65	0.35	0	0	0.50	0.50
	473	0.3[a]	0.7[a]	0[a]	0.32	0.68	0	—	—	—
	573	0	0.66[a]	0.33[a]	0	0.44	0.56	0	0.36	0.64
	673	0	0.5[a]	0.5[a]	0	0	1.0	0	0	1
1.8% Cu/GF-IE	423	0.13	0.21	0.66	0	0.24	0.76	0	0.05	0.95
	473	0	0	1	0	0	1.0	0	0	1.0
	573	0	0	1	0	0	1.0	0	0	1.0
	673	0	0	1	0	0	1.0	0	0	1.0

[a] Based on total CO uptake.

present study is attributed to the greater dispersion of Cu on AC-HNO_3, presumably via the formation of Cu carboxylate species, as indicated by the DRIFT spectra of these samples. In a study of Pd/C catalysts by Morikawa *et al.* (78), the formation of palladiumamine complex cations via proton exchange with carboxylic acid groups on an oxidized carbon support was found to be effective for the decomposition and easy reduction to metallic Pd. Recently, the effect was again observed for a similar catalyst (77) in which Pd deposited on a carbon surface subjected to HNO_3 treatment prior to Pd impregnation was found to reduce easily at about 373 K. Similar to this behavior, the formation of Cu carboxylate species in this study might be responsible for greater dispersion and consequently easier reduction to Cu^0 on AC-HNO_3. The absence of these surface species on Cu/AC-HTT-H_2 results in a lower dispersion, and substantially higher temperatures are required to reduce the larger Cu oxide particles.

Alternatively, one can speculate that the effect can also be rationalized on the basis of electrostatic repulsive forces at the surface of AC-HNO_3. Cu crystallites on AC-HNO_3 are surrounded by electron-rich oxygen-containing groups. Close proximity between these functional groups and Cu oxide lattice oxygens could give rise to electrostatic repulsive forces on the carbon surface, constituting a driving force that could facilitate easier removal of "O" from Cu lattices on AC-HNO_3. On the other hand, no such forces could be envisioned to exist on the surface of AC-HTT-H_2, resulting in CuO crystallites with a reduction profile similar to that of bulk CuO. The observations by Robertson *et al.*, who compared the reducibility of bulk CuO with that of CuO dispersed on SiO_2, could also be interpreted in terms of similarly enhanced "O" removal from supported CuO. Although no additional evidence is available to further substantiate this explanation, it does provide a rationale that can help differentiate between surface and bulk reducibilities.

Similar to the AC-supported samples, the data obtained with Cu/DM and Cu/GF-WI from the three different techniques are quite consistent with each other and support the earlier argument that Cu reducibility is dependent on the crystallite size to some extent. Based on the infrared peak assignments discussed elsewhere (67), those at 2120 and 2158 cm^{-1} in the DRIFT spectra of CO adsorbed at 173 K on Cu/DM (Fig. 15) can be assigned to CO on Cu^+ and Cu^{2+} species, respectively. Thus there is a mixture of Cu^{2+} and Cu^+ surface species on DM-supported Cu after the calcination step. Autoreduction during the partial decomposition of the nitrate precursor at this low calcination temperature could be responsible for the generation of these cuprous species, as observed previously (85–89). After reduction at 423 K, a small fraction of the cupric form is still retained, with the rest of the Cu surface being in the cuprous state. Reduction at 473 K yields a uniform surface covered with Cu^+ species. Increasing the reduction temperature to 573 K converts a significant fraction of these Cu^+ species to metallic

Cu, as evident by the appearance of the new strong band at 2110 cm^{-1}; however, complete reduction of all surface Cu species to metallic Cu appears to occur only after reduction at 673 K, as depicted by the single strong band at 2111 cm^{-1}. The possible weak shoulder on the high wavenumber side could be due to stabilization of CO on isolated Cu^0 sites on the support. Thus, the degree of difficulty encountered in reducing Cu dispersed on DM is similar to that observed in the case of Cu/AC-HTT-H_2, and Table 3 indicates that these two catalysts have comparable Cu dispersions. Cu deposited on GF via a wet impregnation technique, which gave a much lower dispersion compared with the other catalysts, is much more stable and difficult to reduce than the other catalysts. This behavior exhibited by Cu could be indicative of a unique complication encountered when optimizing carbon surfaces for supported Cu catalysts and further endorses the importance of carbon surface chemistry in determining the behavior of metal/carbon catalysts (1). A comprehensive study of the catalytic properties of these catalysts indicated that the presence of both Cu^+ and Cu^0 species is required to achieve the highest activity and stability (58). Whereas a higher Cu dispersion would be desirable to enhance Cu surface area, a lower dispersion will apparently lead to a better stabilization of Cu in the cuprous form on a relatively inert support. An optimum choice of the support, the pretreatment, and the precursor solution could lead to a catalyst with higher dispersion but with "unaccelerated" reducibility of Cu. For example, impregnation of the hydrophobic AC-HTT-H_2 with copper acetate in ethanol could perhaps render such an optimum catalyst formulation. Although this behavior might change as the Cu loading is varied, all these factors would have to be taken into account from a commercial point of view when optimizing the pretreatment conditions.

Additional interaction with the support can also lead to modifications in the morphological and electronic properties of very small Cu crystallites which can result in deviations from the general behavior depicted above, as illustrated by the Cu/GF-IE catalyst. With XRD patterns indicating the presence of 40- to 50-nm Cu^0 particles and chemisorption indicating an average particle size of 2–3 nm, it is possible that a large fraction of these particles are actually smaller than the surface average size predicted by assuming a uniform particle morphology. Perturbations in the electronic structure of Cu on graphitic carbon supports as the cluster size is decreased have been observed before by various spectroscopic studies of this system (11–15). Whereas the peak corresponding to CO stabilized on metallic Cu is around 2100 cm^{-1} in the DRIFT spectra of all other catalysts, it is red-shifted to around 2060 cm^{-1} in the case of Cu/GF-IE. This lower-wavenumber IR band associated with stabilization of CO on Cu^0 may indicate an enhancement in the electron density of the hybrid $d+s$ valence bands of these Cu^0 particles, which can be explained by considering the nature of CO bonding with transition metals in terms of a σ–π bonding model (68). According to this model, CO bonding with Cu involves the delocalization of the CO 5σ-electron pair to unoccupied hybrid $d+s$ orbitals of the adsorption sites (σ bonding) and electron transfer from the occupied d orbitals of the corresponding symmetry to the 2π antibonding orbitals of CO (π bonding). The stretching vibration frequency in the adsorbed CO complexes will depend on the relative contributions of σ and π bonding which, in turn, depend on the state of the adsorption site. For Cu^{2+} ions, the contribution of π bonding is relatively small and CO adsorption involves mainly σ bonding, which leads to an increase in the frequency of vibration. On the other hand, for metallic Cu with no valence vacancies, a significant role is played by π bonding, which increases the electron density in the antibonding orbitals of CO and results in a strong shift to lower frequency. A further increase in the charge density of Cu, as proposed in the above model, should then enhance the contribution due to the π bonding and shift the vibration frequency to still lower values. Such an enhancement in the electron density of these smaller crystallites might be indicative of an electronic interaction between Cu and the graphitized fibers, as suggested by Richard and co-workers for Pt/graphite (23–25). This interaction could be due to an electron delocalization from the center of the polyaromatic rings in the graphite basal planes toward the periphery where these Cu particles are located, with or without the participation of electron-donor "O" groups located at the edges and steps of these basal planes. The low IR band frequency may also be indicative of the presence of a large fraction of Cu(111) index planes in these crystallites (69). Flat Pt particles deposited on supports like graphite on which epitaxy can occur have also been shown by electron microscopy to be usually represented by the (111) crystal plane to a large extent (90). Since both Cu and Pt have fcc-centered lattice structures, by analogy an identical situation could be envisioned for small Cu particles deposited along the edges and adlayers of the graphitic basal planes. Although no other experimental evidence is available to further support these modifications proposed for Cu deposited on GF by ion exchange, they do provide one explanation for the unique adsorption and catalytic properties exhibited by this catalyst (58).

SUMMARY

Cu crystallites dispersed on different forms of carbon, i.e., activated carbon, graphitized carbon fibers, and diamond, were prepared and characterized by CO chemisorption, N_2O decomposition, X-ray diffraction, transmission electron microscopy, temperature-programmed reduction, and DRIFTS. Increasing the concentration of oxygen-containing groups on the surface of the activated carbon

by a nitric acid treatment prior to Cu impregnation was beneficial in terms of rendering a higher dispersion of Cu. A higher dispersion of Cu was obtained with the diamond support compared with the graphitized fibers when prepared via a wet impregnation technique, and it is attributed to the stabilization of Cu through interactive "dangling" bonds on the diamond surface. Cu dispersed by an ion-exchange method was stabilized on the graphitized fibers in two morphologically different forms: aggregates of globular particles deposited on top of graphitic basal planes and relatively smaller crystallites at the edges and defects within these planes. These morphological differences enhanced the reducibility of these particles and may have altered the electronic properties of these crystallites.

ACKNOWLEDGMENT

Financial support for this study was provided by the National Science Foundation via Grant CTS-9415335.

REFERENCES

1. Radovic, L. R., and Rodriguez-Reinoso, F., *Chem. Phys. Carbon* **25**, 243 (1997).
2. Stiles, A. B., "Catalyst Supports and Supported Catalysts." Butterworths, Boston, 1987.
3. Cameron, D. S., Cooper, S. J., Dodgson, I. L., Harrison, B., and Jenkins, J. W., *Catal. Today* **7**, 113 (1990).
4. Radovic, L. R., and Sudhakar, C., *in* "Introduction to Carbon Technologies" (H. Marsh, E. A. Heintz, and F. Rodriguez-Reinoso, Eds.). Univ. of Alicante Press, Alicante, Spain, 1996.
5. Bird, A. J., *in* "Catalyst Supports and Supported Catalysts" (A. B. Stiles, Ed.). Butterworths, Boston, 1987.
6. Augustine, R. L., "Heterogeneous Catalysis for the Synthetic Chemist." Marcel Dekker, New York, 1996.
7. Rodriguez-Reinoso, F., *in* "Porosity in Carbons: Characterization and Applications" (J. W. Patrick, Ed.). Edward Arnold, London, 1995.
8. Ehrburger, P., *Adv. Colloid. Interface Sci.* **7**, 275 (1984).
9. Juntgen, H., *Fuel* **65**, 1436 (1986).
10. Leon y Leon, C. A., and Radovic, L. R., *Chem. Phys. Carbon* **24**, 213 (1996).
11. Baetzold, R. C., *Surf. Sci.* **36**, 123 (1972).
12. Carley, A. F., Rajumon, M. K., and Roberts, M. W., *J. Solid State Chem.* **106**, 156 (1993).
13. Jirka, I., *Surf. Sci.* **232**, 307 (1990).
14. De Crescenzi, M., Diociaiuti, M., Lozzi, L., Picozzi, P., Santucci, S., Battistoni, C., and Mattogno, G., *Surf. Sci.* **178**, 282 (1986).
15. Srinivasan, R., and Gopalan, P., *Surf. Sci.* **338**, 31 (1995).
16. Noronha, F. B., Schmal, M., Nicot, C., Moraweck, B., and Frety, R., *J. Catal.* **168**, 42 (1997).
17. Guerrero Ruiz, A., Lopez Gonzalez, J. D., and Rodriguez Ramos, I., *J. Chem. Soc. Chem. Commun.*, 1681 (1984).
18. Phillips, J., Clausen, B., and Dumesic, J. A., *J. Phys. Chem.* **84**, 1814 (1980).
19. Medina, F., Salagre, P., Sueiras, J. E., and Fierro, J. L. G., *Appl. Catal. A* **99**, 115 (1993).
20. Nedorezova, P. M., Saratovskikh, S. L., Kolbanev, I. V., Tsvetkova, V. I., Babkina, O. N., and D'yachkovskii, F. S., *Kinet. Catal.* **31**, 151 (1990).
21. Self, V. A., and Sermon, P. A., *J. Chem. Soc. Chem. Commun.*, 834 (1990).
22. Takasu, Y., Sakuma, T., and Matsuda, Y., *Chem. Lett.*, 1179 (1985).
23. Richard, D., and Gallezot, P., *in* "Preparation of Catalysts IV" (B. Delmon, P. Grange, P. A. Jacobs, and G. Poncelet, Eds.), p. 71. Elsevier, Amsterdam, 1987.
24. Giroir-Fendler, A., Richard, D., and Gallezot, P., *in* "Heterogeneous Catalysis and Fine Chemicals" (M. Guisnet, *et al.*, Eds.), p. 171. Elsevier, Amsterdam, 1988.
25. Richard, D., Gallezot, P., Neibecker, D., and Tkatchenko, I., *Catal. Today* **6**, 171 (1989).
26. Yeung, K. L., and Wolf, E. E., *J. Vac. Sci. Technol. B* **9**, 798 (1991).
27. Vannice, M. A., and Garten, R. L., *J. Catal.* **56**, 236 (1979).
28. Kuwahara, M., Ogawa, S., and Ichikawa, S., *Surf. Sci.* **344**, L1259 (1995).
29. Fournier, J., Brossard, L., Tilquin, J., Cote, R., Dodelet, J., Guay, D., and Menard, H., *J. Electrochem. Soc.* **143**, 919 (1996).
30. Imai, J., Suzuki, T., and Kaneko, K., *Catal. Lett.* **20**, 133 (1991).
31. Mahmood, T., Williams, J. O., Miles, R., and McNicol, B. D., *J. Catal.* **72**, 218 (1981).
32. Savoia, D., Trombini, C., and Umani-Ronchi, A., *Pure Appl. Chem.* **57**, 1887 (1985).
33. Baker, R. T. K., Prestridge, E. B., and Garten, R. L., *J. Catal.* **56**, 390 (1979).
34. Atamny, F., Duff, D., and Baiker, A., *Catal. Lett.* **34**, 305 (1995).
35. Lineares-Solano, A., Rodriguez-Reinoso, F., de Lecea, C. S. M., Mahajan, O. P., and Walker, P. L., Jr., *Carbon* **20**, 177 (1982).
36. Ehrburger, P., Mahajan, O. P., and Walker, P. L., Jr., *J. Catal.* **43**, 61 (1976).
37. Schlogl, R., Bowen, P., Millward, G. R., Jones, W., and Boehm, H. P., *J. Chem. Soc. Faraday Trans.* **1**, 1793 (1983).
38. Parkash, S., Chakrabarttup, S. K., and Hooley, J. G., *Carbon* **16**, 231 (1978).
39. Schlogl, R., *in* "Handbook of Heterogeneous Catalysis" (G. Ertl, H. Knözinger, and J. Weitkamp, Eds.), p. 138. Wiley–VCH, Weinheim.
40. Lambrecht, W. R. L., *Physica B* **185**, 512 (1993).
41. Pepper, S. V., *J. Vac. Sci. Technol.* **20**, 643 (1982).
42. Ryndin, Y. A., Alekseev, O. S., Simonov, P. A., and Likhilobov, V. A., *J. Mol. Catal.* **55**, 109 (1989).
43. Ryndin, Y. A., Nogin, Y. N., Paukshtis, E. A., Kalinkin, A. V., Chuvilin, A. L., and Zverev, Y. B., *J. Mol. Catal.* **62**, 45 (1990).
44. Ryndin, Y. A., Alekseev, O. S., Paukshtis, E. A., Zaikovskii, V. I., and Kalinkin, A. V., *J. Mol. Catal.* **68**, 355 (1991).
45. Bialas, H., and Niess, J., *Thin Solid Films* **268**, 35 (1995).
46. Baumann, P. K., and Nemanich, R. J., *Appl. Surf. Sci.* **104**, 267 (1996).
47. Bradley, R. H., *Appl. Surf. Sci.* **90**, 271 (1995).
48. Chen, P. A., *Thin Solid Films* **204**, 413 (1991).
49. Grzybek, T., *Pol. J. Chem.* **67**, 335 (1993).
50. Kato, A., Matsuda, F., Nakajima, F., Imanari, M., and Watanabe, Y., *J. Phys. Chem.* **85**, 1710 (1981).
51. Gao, Z., and Wu, Y., *React. Kinet. Catal. Lett.* **59**, 359 (1996).
52. Nishijima, A., Kiyozumi, Y., Ueno, A., Kurita, M., Hagiwara, H., Sato, T., and Todo, N., *Bull. Chem. Soc. Japan* **52**, 3724 (1979).
53. Singoredjo, L., Slagt, M., Wees, J., Kapteijn, F., and Moulijn, J. A., *Catal. Today* **7**, 157 (1990).
54. Barnes, P. A., Dawson, E. A., and Midgley, G., *J. Chem. Soc. Faraday Trans.* **88**, 349 (1992).
55. Barnes, P. A., and Dawson, E. A., *J. Thermal Anal.* **41**, 621 (1994).
56. Rao, R., Dandekar, A., Baker, R. T. K., and Vannice, M. A., *J. Catal.* **171**, 406 (1997).
57. Dandekar, A., Baker, R. T. K., and Vannice, M. A., *Carbon* **36**, 1821 (1998).
58. Dandekar, A., Baker, R. T. K., and Vannice, M. A., submitted for publication. (Pt. II)
59. Krishnakutty, N., and Vannice, M. A., *J. Catal.* **155**, 312 (1995).
60. Bansal, R. C., Vastola, F. J., and Walker, P. L., Jr., *J. Colloid Interface Sci.* **32**, 187 (1970).

61. Kohler, M. A., Lee, J. C., Trimm, D. L., Cant, N. W., and Wainwright, M. S., *Appl. Catal.* **31**, 309 (1987).
62. Dandekar, A., Ph.D. dissertation, Pennsylvania State University, 1998.
63. Na, B. K., Walters, A. B., and Vannice, M. A., *Appl. Spectrosc.* **140**, 585 (1993).
64. Chinchen, G. C., Hay, C. M., Vandervell, M. D., and Waugh, K. C., *J. Catal.* **103**, 79 (1987).
65. Venter, J. J., and Vannice, M. A., *Appl. Spectrosc.* **42**, 1096 (1988).
66. Fanning, P. E., and Vannice, M. A., *Carbon* **31**, 721 (1993).
67. Dandekar, A., and Vannice, M. A., *J. Catal.* **178**, 621 (1998).
68. Davydov, A. A., "Infrared Spectroscopy of Adsorbed Species on the Surface of Transition Metal Oxides." Wiley, London, 1990.
69. Choi, K. I., and Vannice, M. A., *J. Catal.* **131**, 22 (1991).
70. Park, S. H., McClain, S., Tain, Z. R., Suib, S. L., and Karwacki, C., *Chem. Mater.* **9**, 176 (1997).
71. Stoch, J., and Gablankowska-Kukucz, J., *Surf. Interface Anal.* **17**, 165 (1991).
72. Desimoni, E., Casella, G. I., Salvi, A. M., Catadi, T. R. I., and Morone, A., *Carbon* **30**, 527 (1992).
73. Morra, M., Occhiello, E., and Garbassi, F., *Surf. Interface Anal.* **16**, 412 (1990).
74. Parmigiani, F., Pacchioni, G., Illas, F., and Bagus, P. S., Jr., *J. Electron Spectrosc. Relat. Phenom.* **59**, 255 (1992).
75. Socrates, G., "Infrared Characteristic Group Frequencies." Wiley, Chichester, 1980.
76. Colthup, N. B., Daly, L. H., and Wiberley, S. E., "Introduction of Infrared and Raman Spectroscopy," 3rd ed. Academic Press, San Diego.
77. Suh, D. J., Park, T., and Ihm, S., *Carbon* **31**, 427 (1993).
78. Morikawa, K., Shirasaki, T., and Okada, M., *Adv. Catal.* **20**, 97 (1969).
79. Ma, J., Rodriquez, N. M., Vannice, M. A., and Baker, R. T. K., *J. Catal.*, in press.
80. Prado-Burguete, C., Linares-Solano, A., Rodriguez-Reinoso, F., and Salinas-Martinez De Lecea, C., *J. Catal.* **115**, 98 (1989).
81. Ehrburger, P., Mongilardi, A., and Lahaye, J., *J. Colloid Interface Sci.* **21**, 275 (1984).
82. Coloma, F., Sepulveda-Escribano, A., and Rodriguez-Reinoso, F., *Appl. Catal. A* **123**, L1 (1995).
83. Antonucci, P. L., Alderucci, V., Giordano, N., Cocke, D. L., and Kim, H., *J. Appl. Electrochem.* **24**, 58 (1994).
84. Robertson, S. D., Mcnicol, B. D., de Baas, J. H., and Kloet, S. C., *J. Catal.* **37**, 424 (1975).
85. Padley, M. B., Rochester, C. H., Hutchings, G. J., and King, F., *J. Catal.* **148**, 438 (1994).
86. Hadjiivanov, K. I., Kantcheva, M. M., and Klissurski, D. G., *J. Chem. Soc. Faraday Trans.* **92**, 4595 (1996).
87. Shepotko, M., Davydov, A., and Budneva, A., *Kinet. Katal.* **35**, 612 (1994).
88. Pieplu, T., Poignant, F., Vallet, A., Saussey, J., and Lavalley, J. C., *Stud. Surf. Sci. Catal.* **96**, 619 (1995).
89. Amores, G. M. G., Sanchez-Escribano, V., Busca, G., and Lorenzelli, V., *J. Mater. Chem.* **41**, 965 (1994).
90. Yacaman, M. J., and Daminguez, E. J. M., *J. Catal.* **64**, 213 (1980).